

# A Novel Probe of a Glass Forming Liquid: Generalized Compressibility

Hervé M. Carruzzo<sup>†</sup> and Clare C. Yu

*Department of Physics and Astronomy, University of California, Irvine, Irvine, California 92697*  
(December 2, 2024)

We introduce a new quantity to probe the glass transition. This quantity is a linear generalized compressibility which depends solely on the positions of the particles. We have performed a molecular dynamics simulation on a glass forming liquid consisting of a two component mixture of soft spheres in three dimensions. As the temperature is lowered, the generalized compressibility drops sharply at the glass transition, with the drop becoming more and more abrupt as the measurement time increases. At our longest measurement times, the drop occurs approximately at the mode coupling temperature  $T_C$ . Similar behavior is seen with increasing density. The behavior of the linear generalized compressibility is in keeping with the specific heat and the inherent structure energy. Our results are consistent with the kinetic view of the glass transition in which the system falls out of equilibrium, but not with an underlying second order phase transition.

## I. INTRODUCTION

The glass transition is still not well understood despite extensive study. There have been two main theoretical approaches to the problem: dynamic and thermodynamic. Theories in the first category view the glass transition as a kinetic phenomenon characterized by a growing relaxation time and viscosity [1–5]. When the relaxation time exceeds the measurement time, particle motion appears to be arrested resulting in the glass transition. One of the most prominent theories espousing this view is the mode coupling theory (MCT) in which ideally the relaxation time diverges at a temperature  $T_C$  above the experimental glass transition temperature [3]. Interesting and fruitful concepts such as dynamic inhomogeneities [4,6,7] and the influence of the energy landscape on relaxation processes [8,9] have resulted from this approach. The thermodynamic viewpoint attributes the glass transition to an underlying phase transition hidden from direct experimental observation by extremely long relaxation times [1,2,10–12]. In most scenarios there is an underlying second order phase transition associated with a growing correlation length which produces diverging relaxation times as well as diverging static susceptibilities [13–18]. More recently Mezard and Parisi [19,12] have argued that the underlying transition is actually a random first order transition signaled by a jump discontinuity in the specific heat.

Experimentally the glass transition is characterized by both kinetic and thermodynamic features. For example in the supercooled liquid kinetic quantities such as the viscosity and relaxation time grow rapidly as the temperature is lowered. When the system falls out of equilibrium below a certain temperature, thermodynamic quantities exhibit features reflecting the glass transition. For example as the system is cooled the specific heat has a step-like form and the dielectric constant exhibits a peak

at a frequency dependent temperature.

In an effort to better characterize the glass transition we introduce a novel probe which we call a generalized compressibility [20]. Unlike the specific heat which monitors energy fluctuations, this linear compressibility is a function of the microscopic structure of the system: it depends solely on the positions of the particles and not on their previous history. Since we do not need to compare the system's state at different times, it is not a dynamic or kinetic quantity. Rather it is a thermodynamic quantity in the sense that it is purely a function of the microstate of the system dictated by its location in phase space. The generalized compressibility is easy to compute numerically, and it is simpler than the dielectric constant which involves both the translation and orientation of electric dipoles. It should be directly measurable experimentally in colloidal suspensions of polystyrene spheres [21] and possibly in other systems as well. In this paper we present measurements of this quantity in a molecular dynamics simulation of a two component system of soft spheres. We find that the linear generalized compressibility drops sharply as the temperature decreases below the glass transition temperature  $T_g$ . The drop becomes more and more abrupt as the measurement time increases. This is consistent with the structural arrest associated with a kinetic transition in which the system falls out of equilibrium.

The paper is organized as follows. Section II describes the molecular dynamics simulations. Section III defines the measurements that were made, i.e., the linear and nonlinear generalized compressibilities, the specific heat, the diffusion constant and the intermediate scattering function. Section IV gives the results for the crystal while section V gives the results for the glass forming liquid as a function of temperature and density. Finally we discuss our results in Section V.

## II. MOLECULAR DYNAMICS SIMULATION

We have performed a molecular dynamics simulation on a glass forming liquid [22,23] consisting of a 50:50 binary mixture of soft spheres in three dimensions. The two types of spheres, labelled A and B, differ only in their sizes. The interaction between two particles a distance  $r$  apart is given by  $V_{\alpha\beta}(r) = \epsilon[(\sigma_{\alpha\beta}/r)^{12} + X_{\alpha\beta}(r)]$  where the interaction length  $\sigma_{\alpha\beta} = (\sigma_\alpha + \sigma_\beta)/2$  with  $\sigma_B/\sigma_A = 1.4$  ( $\alpha, \beta = A, B$ ). For numerical efficiency, we set the cutoff function  $X_{\alpha\beta}(r) = r/\sigma_{\alpha\beta} - \lambda$  with  $\lambda = 13/12^{12/13}$ . The interaction is cutoff at the minimum of the potential  $V_{\alpha\beta}(r)$ . Energy and length are measured in units of  $\epsilon$  and  $\sigma_A$ , respectively. Temperature is given in units of  $\epsilon/k_B$  where  $k_B$  is Boltzmann's constant, and time is in units of  $\sigma_A\sqrt{m/\epsilon}$  where  $m$ , the mass of the particles, is set to unity. The equations of motion were integrated using the leapfrog method [24] with a time step of 0.005. During each run the average density  $\rho_o = N/L^3$  was fixed, and the temperature was kept constant using a constraint algorithm [24]. The volume  $V = L^3$ .  $N = N_A + N_B$  is the total number of particles. The system occupies a cube with dimensions  $(\pm L/2, \pm L/2, \pm L/2)$  and periodic boundary conditions.

We have done sweeps of both temperature and density. For the temperature sweeps, we fix the density and perform the following measuring procedure. For runs where we cool the system, we start each run at a high temperature ( $T=1.5$ ) and lower the temperature in steps of  $\Delta T = 0.05$ . At each temperature we equilibrate for  $10^4$  molecular dynamics steps (md steps) and then measure the quantities of interest for  $N_\tau$  additional md steps where  $N_\tau = 10^5, 2 \times 10^5, 10^6, 3 \times 10^6$ , or  $10^7$ . All the particles move at each md step. The results are then averaged over up to 40 different initial conditions (different initial positions and velocities of the spheres). We have done some runs in which we heat the system of particles by starting at our lowest temperature  $T = 0.1$  with a configuration obtained by cooling the system. We then increased the temperature in steps of  $\Delta T = 0.05$ . As before we equilibrate at each temperature for  $10^4$  time steps and then measure quantities for an additional  $10^6$  time steps.

We have also done some density sweeps in which we fix the temperature ( $T=1.0$ ) and systematically change the density. The glass transition occurs as we increase the density. Colloidal experiments often study the glass transition as a function of density. We start each run at a low density ( $\rho = 0.4$ ) and increase the density in steps of  $\Delta\rho = 0.025$  in md units. At each density we equilibrate for  $10^4$  md steps and then measure the quantities of interest for  $N_\tau$  additional md steps.

The glass transition occurs either as the temperature is lowered or as the density is raised. It is worth noting that temperature and density can be combined into

a dimensionless parameter  $\Gamma$  [25]:

$$\Gamma = \rho\sigma_{eff}^3/T^{\frac{1}{4}} \quad \sigma_{eff}^3 = \sum_{\alpha\beta} n_\alpha n_\beta \sigma_{\alpha\beta}^3 \quad (1)$$

where  $\sigma_{eff}$  represents an effective diameter for particles in the mixture. The concentration of each type of particle is given by  $n_A = N_A/N$  and  $n_B = 1 - n_A$ . For our simulations  $n_A = n_B = 0.5$ .  $\Gamma$  is the relevant parameter when the particles spend most of their time sampling a nonzero interparticle potential, i.e., for  $\rho^{-1/3} < \sigma_{eff}$ . Thus  $\Gamma$  is particularly useful for interparticle interactions which fall off with distance as a power law and do not have a cutoff beyond which the interaction is zero. When cooling from the liquid phase, the glass transition is known to occur around  $\Gamma = 1.45$  [25].

## III. MEASUREMENTS

### A. Generalized Compressibilities

We now derive expressions for the linear and nonlinear generalized compressibility. To probe the density fluctuations, we follow the approach of linear response theory and consider applying an external potential  $\frac{\Delta P}{\rho_o}\phi(\vec{r})$  which couples to the local density  $\rho(\vec{r}) = \sum_{i=1}^N \delta(\vec{r} - \vec{r}_i)$  where  $\vec{r}_i$  denotes the position of the  $i^{th}$  particle.  $\rho_o$  is the average density.  $\Delta P$  has units of pressure and sets the magnitude of the perturbation.  $\phi(\vec{r})$  is a dimensionless function of position that must be compatible with the periodic boundary conditions imposed on the system, i.e., it must be continuous across the boundaries, but is otherwise arbitrary. This adds to the Hamiltonian  $H$  of the system a term

$$U = \frac{\Delta P}{\rho_o} \int_V d^3r \phi(\vec{r}) \rho(\vec{r}) = \frac{\Delta P}{\rho_o} \sum_i \phi(\vec{r}_i) \equiv \frac{\Delta P}{\rho_o} \rho_\phi \quad (2)$$

where we have defined  $\rho_\phi = \int_V d^3r \phi(\vec{r}) \rho(\vec{r}) = \sum_i \phi(\vec{r}_i)$ .  $\rho_\phi$  is the inner product of  $\phi$  and  $\rho(\vec{r})$ , and we can regard it as a projection of the density onto a basis function  $\phi(r)$ , i.e.,  $\rho_\phi = \langle \rho | \phi \rangle$ . It weights the density fluctuations according to their spatial position. The application of the external potential will induce an average change  $\delta\rho_\phi$  in  $\rho_\phi$ :

$$\delta\rho_\phi = \langle \rho_\phi \rangle_U - \langle \rho_\phi \rangle_{U=0} \quad (3)$$

where the thermal average  $\langle \rho_\phi \rangle_U$  is given by

$$\langle \rho_\phi \rangle_U = \frac{1}{Z} \text{Tr} \left[ e^{-\beta(H+U)} \rho_\phi \right] \quad (4)$$

The partition function  $Z = \text{Tr} e^{-\beta(H+U)}$  and  $\beta$  is the inverse temperature. For small values of  $\Delta P$ , this change can be calculated using perturbation theory [26]. Up to third order in  $\Delta P$ , we find

$$\delta\rho_\phi = -\frac{\beta\Delta P}{\rho_o}\langle\rho_\phi^2\rangle_c + \frac{\beta^2\Delta P^2}{2\rho_o^2}\langle\rho_\phi^3\rangle_c - \frac{\beta^3\Delta P^3}{6\rho_o^3}\langle\rho_\phi^4\rangle_c, \quad (5)$$

where the cumulant averages are

$$\langle\rho_\phi^2\rangle_c = \langle\rho_\phi^2\rangle - \langle\rho_\phi\rangle^2 \quad (6)$$

$$\langle\rho_\phi^3\rangle_c = \langle\rho_\phi^3\rangle - 3\langle\rho_\phi\rangle\langle\rho_\phi^2\rangle + 2\langle\rho_\phi\rangle^3 \quad (7)$$

$$\langle\rho_\phi^4\rangle_c = \langle\rho_\phi^4\rangle - 4\langle\rho_\phi\rangle\langle\rho_\phi^3\rangle - 3\langle\rho_\phi^2\rangle^2 + 12\langle\rho_\phi\rangle^2\langle\rho_\phi^2\rangle - 6\langle\rho_\phi\rangle^4 \quad (8)$$

with the thermal average  $\langle\rho_\phi^n\rangle = \langle\rho_\phi^n\rangle_{U=0}$ . The third order cumulant, eq.(7), is zero in the liquid phase because for every configuration there exists an equivalent configuration with the opposite sign of  $(\rho_\phi - \langle\rho_\phi\rangle)$  and so we will not consider this term any further. We can recast eq. (5) as a power series in the perturbation  $\Delta P$ :

$$\frac{\delta\rho_\phi}{N} = -\frac{1}{6\rho_o k_B T}\chi_l\Delta P + \frac{1}{6(\rho_o k_B T)^3}\chi_{nl}(\Delta P)^3 \quad (9)$$

where

$$\chi_l = \frac{6}{N}\langle(\rho_\phi)^2\rangle_c \quad \chi_{nl} = -\frac{1}{N}\langle(\rho_\phi)^4\rangle_c. \quad (10)$$

In the remainder of this paper we will focus our attention on the linear ( $\chi_l$ ) and nonlinear ( $\chi_{nl}$ ) dimensionless generalized compressibilities defined by the above expressions. We now discuss the choice of the function  $\phi$ . We consider applying the potential along the direction  $\mu$  of one of the coordinate axes so that  $\phi(\vec{r}) = \phi(r^\mu)$ . A natural candidate for  $\phi(r^\mu)$  is  $\cos(k_\mu r^\mu)$  (no implied sum over repeated indices) with  $k_\mu = 2\pi n/L$ , where  $n = 1, 2, \dots$ . In this case,  $\rho_\phi$  is the  $k^{th}$  mode of the cosine transform of the density. We will also consider the simpler function  $\phi(r^\mu) = |r^\mu|/L$ . The absolute value corresponds to the case where all the particles feel a force along the  $\mu$ th direction pointing towards the origin. It gives results very similar to  $\phi(r^\mu) = \cos(k_\mu r^\mu)$  for small  $k$  at a fraction of the computational cost. (No sum over repeated indices.) So our results in this paper correspond to two cases:

$$\rho_\phi = \sum_i |r_i^\mu|/L \quad (11)$$

which is rather like a center of mass, and

$$\rho_\phi = \sum_i \cos(k_\mu r_i^\mu) \quad (12)$$

Since the system is isotropic, we compute the compressibilities for each direction and then average over the direction  $\mu$ .

## B. Specific Heat

The specific heat is a thermodynamic quantity which undergoes a change signaling the glass transition. In experimental systems under constant pressure the specific heat exhibits a smooth step down as the temperature is lowered through the glass transition. In our simulations which are done at constant volume, the specific heat has a peak at the glass transition. It is a useful check of our calculation to see if the peak occurs at the same temperature (or density) as the drop in the linear generalized compressibility. There are two ways to compute the specific heat  $C_V$  per particle at constant volume  $V$ . The first is by taking a derivative of the average energy  $\langle E \rangle$  per particle with respect to temperature:  $C_V = d\langle E \rangle/dT$ . Since we study the system at discrete temperatures, we approximate the derivative by a finite difference:

$$C_V(T_n) = \frac{\langle E(T_n) \rangle - \langle E(T_{n-1}) \rangle}{T_n - T_{n-1}} \quad (13)$$

where  $T_n > T_{n-1}$  for all integers  $n$ . The second way to calculate the specific heat is from the fluctuations:

$$C_V = Nk_B\beta^2 (\langle E_P^2 \rangle - \langle E_P \rangle^2) \quad (14)$$

where  $k_B$  is Boltzmann's constant,  $\beta$  is the inverse temperature, and  $E_P$  is the potential energy per particle. In our three dimensional simulations the kinetic energy per particle is given by  $3k_B T/2$ , so it is the fluctuations in the potential energy  $E_P$  per particle which determine the temperature dependence of the specific heat. Thus

$$C_V = \frac{3}{2}k_B + Nk_B\beta^2 (\langle E_P^2 \rangle - \langle E_P \rangle^2) \quad (15)$$

In equilibrium these two ways of calculating the specific heat should agree. So we compare the results of calculating  $C_V$  both ways as a check on our calculation and to make sure the system has equilibrated in all the basins that were visited in the energy landscape.

## C. Diffusion Constant

The diffusion of the particles reflects the kinetics of the system and becomes very small below the crystallization or glass transition temperature. We calculate the diffusion constant  $D$  using the Einstein relation

$$D = \lim_{t \rightarrow \infty} \frac{1}{6Nt} \langle \sum_{i=1}^N (\mathbf{r}_i(t) - \mathbf{r}_i(0))^2 \rangle \quad (16)$$

where  $\mathbf{r}_i$  are true displacements of the  $i$ th particle. Since we are using periodic boundary conditions, if the particle has crossed the box several times, then this must be included in  $\mathbf{r}_i$ .

In principle we can fit  $D(T)$  to the power law form predicted by mode coupling theory in order to determine the mode coupling temperature  $T_C$ . However the more accepted way of determining  $T_C$  is via the intermediate scattering function and so this is how we will determine  $T_C$ .

#### D. Intermediate Scattering Function

The intermediate scattering function  $F(\vec{k}, t)$  is a useful probe of the structural relaxation. It is the spatial Fourier transform of the van Hove correlation function  $G(\vec{r}, t)$  and the inverse time transform of the dynamic structure factor  $S(\vec{k}, \omega)$ . There are two different types of intermediate scattering function: the self (incoherent) intermediate scattering function  $F_s(\vec{k}, t)$  and the full (coherent) intermediate scattering function  $F(\vec{k}, t)$ .

In a computer simulation, the self (incoherent) part of the partial intermediate scattering function  $F_{s,\alpha}(\vec{k}, t)$  can be calculated directly using [27]

$$F_{s,\alpha}(\vec{k}, t) = \frac{1}{N_\alpha} \left\langle \sum_{i=1}^{N_\alpha} e^{i\vec{k} \cdot (\vec{r}_i(t) - \vec{r}_i(0))} \right\rangle \quad (17)$$

where the subscript  $\alpha$  refers to the particle type, A or B.  $\vec{r}_i(t)$  is the position of particle  $i$  at time  $t$ , and  $\langle \dots \rangle$  refers to an average over different configurations. The wavevector  $\vec{k} = 2\pi\vec{q}/L$  where  $\vec{q}$  is a vector of integers. For an isotropic system  $F_{s,\alpha}(\vec{k}, t)$  depends only on the magnitude  $k = |\vec{k}|$ . We will choose  $k = k_{max}$  where  $k_{max}$  is the position of the first maximum of the partial static structure factor  $S_\alpha(k)$ . We define a relaxation time  $\tau_s$  as the time where  $F_{s,\alpha}(\vec{k}, t)$  decays to  $1/e$ . We can determine the mode coupling  $T_C$  by fitting  $\tau_s$  to the form  $\tau_s \sim (T - T_C)^{-\gamma}$ . For the self part of the intermediate scattering function, the actual value of  $\tau_s$  increases as the magnitude of the wavevector decreases [28]. However, the value of  $T_C$  is independent of  $k$ .

The full intermediate scattering function  $F(\vec{k}, t)$  is given by [27]

$$F_\alpha(\vec{k}, t) = \frac{1}{N_\alpha} \left\langle \rho_{\vec{k},\alpha}(t) \rho_{-\vec{k},\alpha}(0) \right\rangle \quad (18)$$

where the Fourier transform of the density  $\rho_{\vec{k}}(t) = \sum_{i=1}^N e^{-i\vec{k} \cdot \vec{r}_i(t)}$ . The subscript  $\alpha$  refers to the particle type, A or B. The longest  $\alpha$  relaxation time can be determined from the full intermediate scattering function evaluated at  $k = k_{max}$  [29]. We will define the  $\alpha$  relaxation time  $\tau$  as the time where  $F_\alpha(k_{max}, t)$  decays to  $1/e$ .

The runs used to determine the intermediate scattering function were done in a slightly different way from the other measurements. These runs were performed at

a given temperature and density for  $N_\tau$  md time steps with no change in temperature or density. The runs were started from a configuration that had been equilibrated at that temperature and density using parallel tempering. The parallel tempering technique is described in the appendix.

#### E. Grand Canonical Ensemble and the Ordinary Isothermal Compressibility

In most of our calculations we will work in the canonical ensemble where we fix the volume  $V$ , the number  $N$  of particles and the density  $\rho_o$ . However, it is straightforward to generalize our results to the grand canonical ensemble where the number of particles is not fixed. We simply replace the thermal average defined in equation (4) by

$$\langle \rho_\phi \rangle_U = \frac{1}{\mathcal{Z}} \sum_N e^{\mu N} \text{Tr} \left[ e^{-\beta(H_N + U_N)} \rho_\phi \right] \quad (19)$$

where  $\mu$  is the chemical potential,  $H_N$  is the Hamiltonian with  $N$  particles,  $U_N$  is given by eq. (2) for a system with  $N$  particles, and  $\mathcal{Z}$  is the grand canonical partition function given by

$$\mathcal{Z} = \sum_N e^{\mu N} \text{Tr} \left[ e^{-\beta(H_N + U_N)} \right] \quad (20)$$

The generalized compressibilities can be defined using equations (7) through (10) with the thermal averages  $\langle \rho_\phi^n \rangle = \langle \rho_\phi^n \rangle_{U=0}$  defined in the grand canonical ensemble.

The ordinary isothermal compressibility  $\kappa_T$  can be related to the fluctuations in the number, volume or density of the system. In most of our calculations we fix the volume, number of particles and density, so that there are no such fluctuations and the system has  $\kappa_T = 0$ . However in the grand canonical ensemble  $\kappa_T$  is given by

$$\kappa_T = \frac{1}{\rho_o k_B T} \frac{\langle N^2 \rangle - \langle N \rangle^2}{\langle N \rangle} \quad (21)$$

where  $\rho_o = \langle N \rangle / V$ . To relate  $\kappa_T$  to the linear generalized compressibility  $\chi_l$ , we choose a uniform potential  $\phi(\vec{r}) = 1$ . Then  $\rho_\phi = \int d^3r \rho(\vec{r}) = N$  and

$$\kappa_T = \frac{1}{6\rho_o k_B T} \chi_l \quad (22)$$

In principle one can also obtain  $\kappa_T$  from the  $k \rightarrow 0$  limit of the static structure factor  $S(\vec{k}) = (1/N) \langle \rho_{\vec{k}} \rho_{-\vec{k}} \rangle$  where  $N$  is the number of particles and  $\rho_{\vec{k}} = \sum_{i=1}^N \exp(-i\vec{k} \cdot \vec{r}_i)$  is the Fourier transform of the local density  $\rho(\vec{r})$ . The limit of  $S(\vec{k})$  for  $k \rightarrow 0$  is [27]

$$S(0) = \rho_o k_B T \kappa_T \quad (23)$$

We chose not to use this approach since there was a slight upturn in the total static structure factor as  $k \rightarrow 0$ , making it difficult to accurately determine  $S(k \rightarrow 0)$  and hence  $\kappa_T$ . This upturn at small  $k$  is due to the contribution of type A particles to  $S(k)$  and can be seen clearly in the partial structure factor  $S_A(k)$ . This is why we choose type B particles in calculating the intermediate scattering function.

#### IV. RESULTS: CRYSTAL

As a point of reference for our calculations and as a way of checking that our program is working properly, we first examine the single component fluid which crystallizes at low temperatures. To this end, we consider a system of 512 identical ( $\sigma_A = \sigma_B$ ) particles at a density  $\rho_o = 1.1$ .

##### A. Specific Heat

In the thermodynamic limit crystallization is associated with a discontinuous jump in the entropy and a delta function in the specific heat. Since we work with finite size systems, the specific heat exhibits a sharp peak as shown in Figure 1. This figure shows the specific heat for 512 particles as a function of temperature where the temperature steps are closely spaced with  $\Delta T = 0.01$  for  $T < 0.7$  and each temperature had a measuring time of  $10^6$  md steps. A sharp delta function-like peak is seen around  $T=0.57$  which corresponds to  $\Gamma = 1.27$ . The low temperature phase ( $T < 0.57$ ) is a crystal with sharp Bragg peaks in the structure factor (not shown).

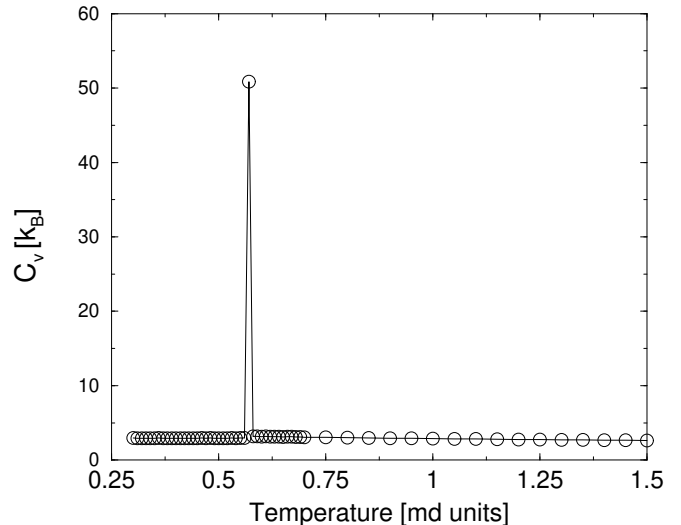


FIG. 1. Specific heat of a one component system as a function of temperature for 512 soft spheres. The delta function signaling crystallization is clearly seen around  $T_m = 0.57$  ( $\rho_o = 1.1$ ). The measurement time was  $10^6$  md steps for each temperature. For  $T < 0.7$  the temperature steps are closely spaced with  $\Delta T = 0.01$  near and below the crystallization temperature. At high temperatures ( $T > 0.7$ ), the temperature steps are spaced with  $\Delta T = 0.05$ . The data shown is for a single cooling run and was calculated from energy fluctuations (eq. (15)).

Upon heating and cooling, the transition shows hysteresis as can be seen in Figure 2. The peak upon heating occurs at a higher temperature than the cooling peak. This is indicative of slight supercooling and superheating. The peaks in the specific heat are not as pronounced as in Figure 1 because the temperature steps ( $\Delta T = 0.05$ ) are farther apart and probably miss the exact temperature where the maximum occurs. In addition averaging over runs smears out the peak which can occur at slightly different temperatures for different runs due to the large temperature steps.

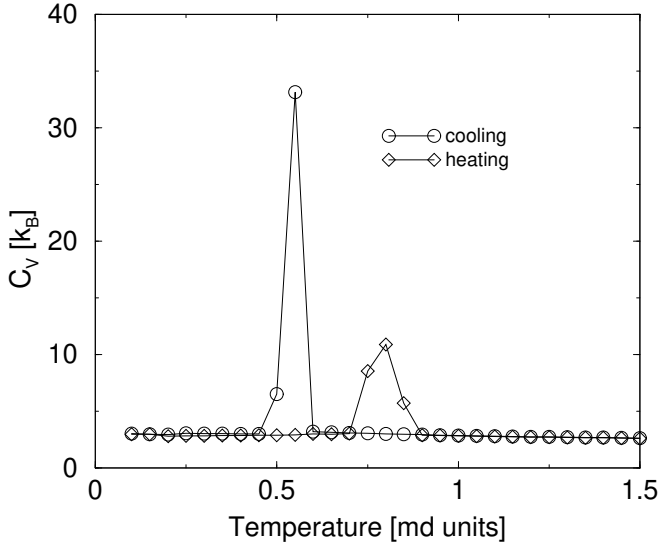


FIG. 2. Specific heat during cooling and heating of a one component system as a function of temperature for 512 soft spheres. Hysteresis is clearly seen.  $\rho_o = 1.1$ . The measurement time was  $10^6$  md steps for each temperature. Energy fluctuations were used to calculate the specific heat. The data shown is averaged over 5 runs.

The hysteresis, the delta function-like peak in the specific heat, and the Bragg peaks are all consistent the fact that crystallization is a first order phase transition.

### B. Generalized Compressibilities and Diffusion Constant

Figure 3 shows the linear compressibility  $\chi_l$  and the diffusion constant  $D$  as a function of temperature for the single component liquid. At high temperatures  $\chi_l$  has a small slope which becomes steeper at low temperatures. The salient feature is the very sharp drop around  $T_m = 0.57$  of the linear generalized compressibility and the diffusion constant. (Recall from the specific heat that the crystallization temperature is around  $T_m = 0.57$ .) The abrupt drop can be seen because the temperature steps are small ( $\Delta T = 0.01$ ). The linear generalized compressibility is calculated using the absolute value scheme of eq. (11).

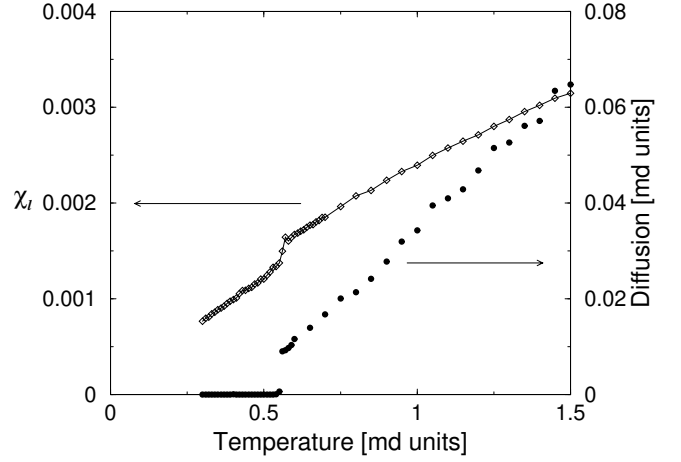


FIG. 3. Linear generalized compressibility and diffusion constant of a one component system as a function of temperature for 512 soft spheres. The crystalline behavior is clearly seen around  $T=0.57$  ( $\rho_o = 1.1$ ). The measurement time was  $10^6$  md steps for each temperature. The compressibility was averaged over 5 runs while the diffusion is shown for a single run.

The diffusion constant showed hysteresis between cooling and heating (see Figure 4). Once again we see that the transition upon heating is at a higher temperature than upon cooling. The larger temperature steps ( $\Delta T = 0.05$ ) and the averaging over runs smear out the abruptness of the transition.

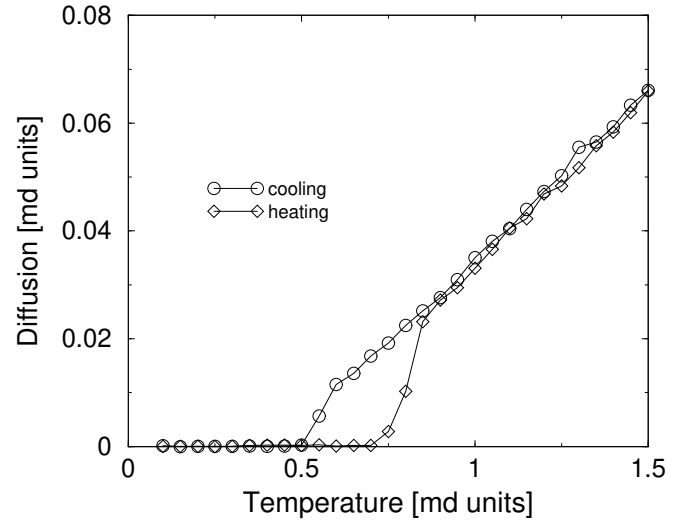


FIG. 4. Diffusion constant of a one component system during cooling and heating shows hysteresis. The measuring time is  $10^6$  md steps. There are 512 single component particles at a density  $\rho_o = 1.1$ . The data is averaged over 5 runs.

The nonlinear compressibility calculated using the absolute value scheme of eq. (11) is shown in Figure 5. Because it is very small and fluctuates in sign, it is zero within the numerical noise.

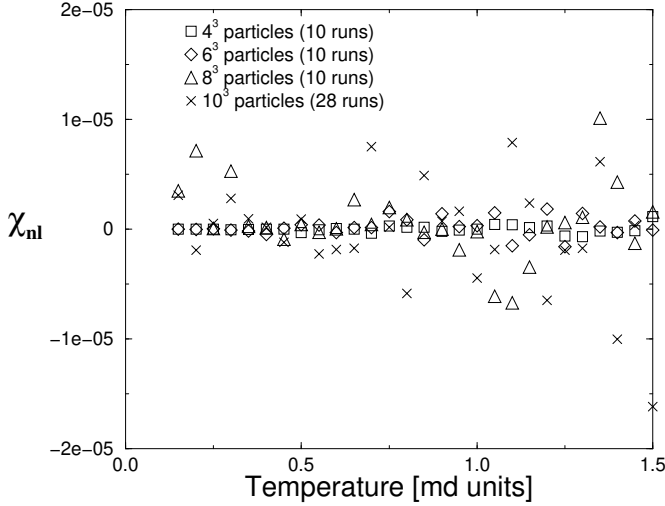


FIG. 5. Nonlinear generalized compressibility of a single component system as a function of temperature. The runs lasted for  $10^5$  md steps. The density  $\rho_o = 1.0$ . The nonlinear compressibility was calculated using the absolute values of the positions of the particles.

## V. RESULTS: GLASS FORMING LIQUID

We now examine the response of the two component glass forming liquid. All the runs in which temperature was varied were done at a density of  $\rho_o = 0.6$  and  $\sigma_B/\sigma_A = 1.4$ . The runs in which density was varied were done at a temperature of  $T = 1$  and  $\sigma_B/\sigma_A = 1.4$ . For these parameters crystallization is avoided upon cooling in both cases.

### A. Intermediate Scattering Function

In Figure 6 we show the self intermediate scattering function  $F_{s,B}(k, t)$  versus time at temperatures below the caging temperature ( $T \approx 0.4$ ). The caging temperature is the highest temperature at which a plateau is present in the intermediate scattering function versus time. The plateau represents the temporary localization of a particle by a cage of other particles surrounding it.

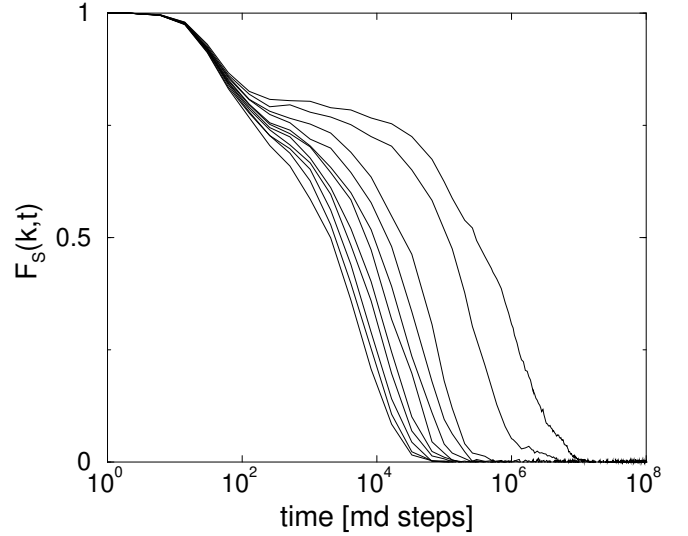


FIG. 6. The self intermediate scattering function versus time for a system with 512 particles and  $\rho_o = 0.6$ . The time is given in units of molecular dynamics time steps. From left to right, the curves are for temperatures  $T = 0.381679, 0.373134, 0.364964, 0.357143, 0.34965, 0.342466, 0.33557, 0.328947, 0.321543, 0.3021148, 0.289855$  respectively. 256 type B particles were used and the wavevector  $k = 2\pi \cdot 8.3666/L$  which is the location of the peak in the structure factor for type B particles.  $L = 8$ . For each curve the system was initialized from a configuration at that temperature obtained from parallel tempering which is described in the Appendix. Then the simulation was run only at that temperature. The temperatures were chosen so that the parallel tempering acceptance rates were high. The curves at the 7 highest temperatures were equilibrated for 1 million md time steps before recording the configurations used to calculate  $F_s(k, t)$ . Each curve of the 7 highest temperature curves is averaged over 24 runs except for  $T = 0.373134$  which is average over 54 runs. The curves for  $T = 0.328947$  and  $0.321543$  were equilibrated for 2 million md time steps before recording the configurations used to calculate  $F_s(k, t)$ . These two curves were averaged over 11 runs. The curve for  $T = 0.3021148$  was averaged over 22 runs and was equilibrated for 10,000 md time steps before recording the configurations used to calculate  $F_s(k, t)$ . The curve for  $T = 0.289855$  was averaged over 36 runs and equilibrated for 50 million md time steps before recording configurations used to calculate  $F_s(k, t)$ .

Mode coupling theory is applicable in the temperature range below the caging temperature and somewhat above the mode coupling  $T_C$ . We define the relaxation time  $\tau_s$  by  $F_s(k, \tau_s) = 1/e$ . We can determine the relaxation times for the seven highest temperatures shown in Figure 6 and then fit the temperature dependence of  $\tau_s(T)$  to the mode coupling form  $\tau_s(T) \sim (T - T_C)^{-\gamma}$ . We find the best fit with the mode coupling temperature  $T_C = 0.303$  which corresponds to  $\Gamma = 1.46$ .  $\tau_s(T)$  versus temperature and the mode coupling fit are shown in Figure 7. Also shown is the fit to the Vogel-Fulcher form  $\tau_s(T) = A \exp[B/(T - T_{VF})]$  with  $T_{VF} = 0.21$  which corresponds to  $\Gamma = 1.60$ . In doing the Vogel-Fulcher fit, we

were able to use a much broader range of temperatures since  $T_{VF}$  is much lower than the mode coupling  $T_C$ .

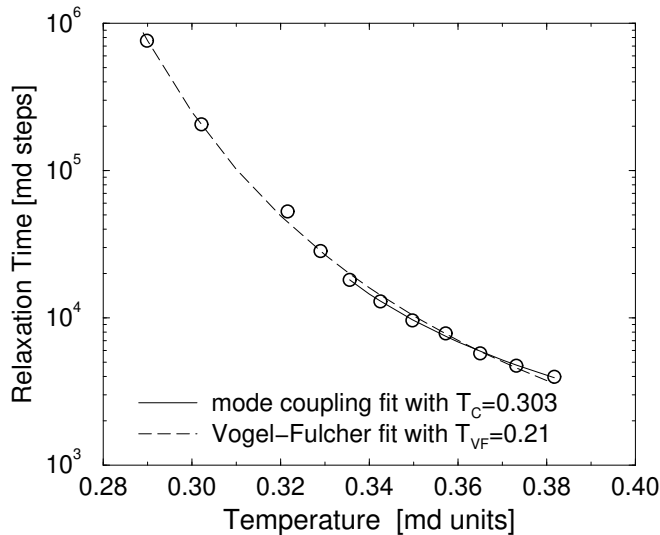


FIG. 7. Relaxation times  $\tau_s$  versus temperature. The solid line is the mode coupling fit to the form  $\tau_s = A(T - T_C)^{-\gamma}$  with  $T_C = 0.303$ ,  $\gamma = 1.735$  and  $A = 47.6$ . The dashed line is the fit to the Vogel-Fulcher form  $\tau_s(T) = A \exp[B/(T - T_{VF})]$  with  $T_{VF} = 0.21$ ,  $A = 33.3$ , and  $B = 0.803$ .

We have also calculated the full intermediate scattering function  $F_B(k, t)$  at a temperature which is just below the mode coupling  $T_C$ . In order to determine the longest  $\alpha$  relaxation time in the vicinity of  $T_C$ , we set  $k = 2\pi \cdot 8.3666/L$  ( $L = 8$ ) which is the location of the peak in the structure factor for type B particles. At  $T = 0.2895858$  we find that  $F_B(k, t)$  has fallen to  $1/e$  at  $\tau = 9.25 \times 10^5$  md time steps for a system with 512 particles of which half are type B. This gives us a time scale by which to compare other times such as our run times. At higher temperatures this relaxation time will be much shorter.

## B. Diffusion Constant

### 1. Diffusion Constant Versus Temperature

As the system is cooled through the glass transition, the diffusion constant calculated using equation (16) becomes negligibly small. This is shown in Figure 8 where the diffusion constant for 512 particles is plotted.

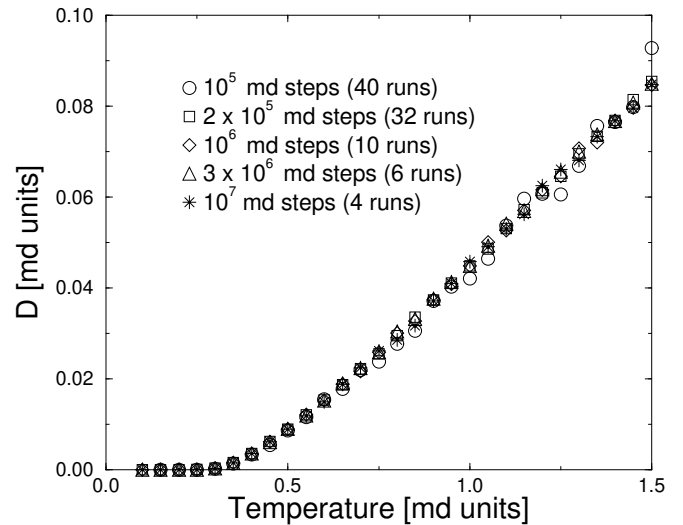


FIG. 8. Diffusion constant as a function of temperature for a binary mixture of 512 particles. Measurement times are  $10^5$ ,  $2 \times 10^5$ ,  $10^6$ ,  $3 \times 10^6$ , and  $10^7$  md steps.  $\rho_o = 0.6$  and  $\sigma_B/\sigma_A = 1.4$ .

The diffusion constant varies smoothly over the entire temperature range. To emphasize that the diffusion constant does not go to zero but just becomes very small, we have replotted the data on a logarithmic scale in Figure 9.

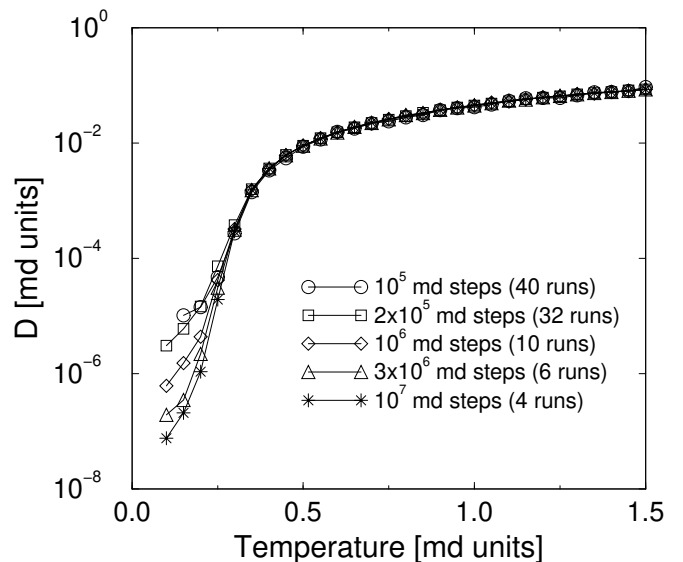


FIG. 9. Diffusion constant as a function of temperature for a binary mixture of 512 particles plotted on a logarithmic scale. Measurement times are  $10^5$ ,  $2 \times 10^5$ ,  $10^6$ ,  $3 \times 10^6$ , and  $10^7$  md steps. Number of runs averaged over is given in the legend.  $\rho_o = 0.6$  and  $\sigma_B/\sigma_A = 1.4$ .

Figure 10 shows the diffusion constant for binary mixtures of several different sizes. The small systems with 64 and 216 particles are a little noisy, but there is no apparent size effect.



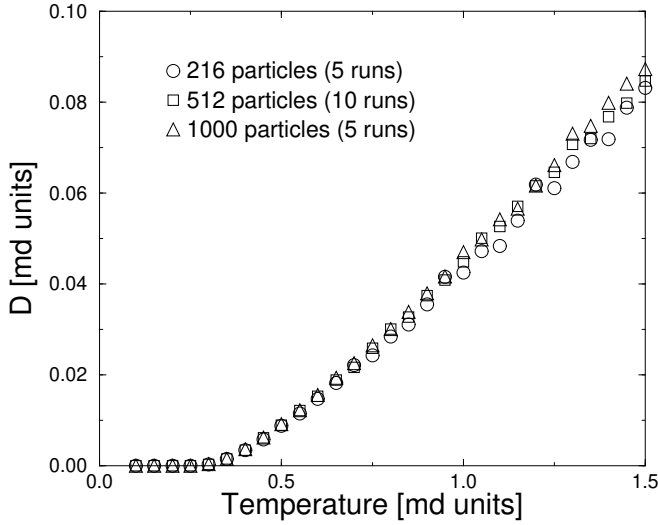


FIG. 10. Diffusion constant as a function of temperature for binary mixtures of 216, 512 and 1000 particles. Measurement time is  $10^6$  md steps.  $\rho_o = 0.6$  and  $\sigma_B/\sigma_A = 1.4$ . Data was averaged over the number of runs indicated in the legend.

## 2. Diffusion Constant Versus Density

In Figure 11 we show the diffusion constant as a function of density. We see that the diffusion goes smoothly to zero as the density  $\rho$  increases.

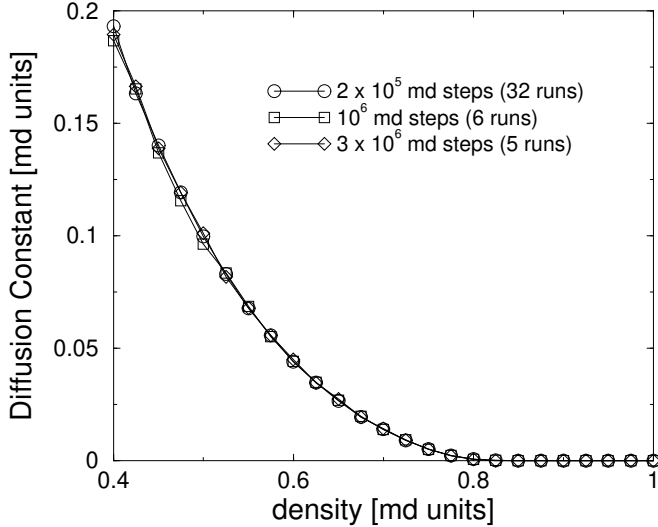


FIG. 11. Diffusion constant as a function of density for a binary mixture of 512 particles at  $T = 1$ . The measurement times are  $2 \times 10^5$ ,  $10^6$  and  $3 \times 10^6$  md steps.  $\sigma_B/\sigma_A = 1.4$ . Data was averaged over the number of runs indicated in the legend.

## C. Specific Heat

### 1. Specific Heat Versus Temperature

The specific heat at constant volume exhibits a peak at the glass transition as shown in Figure 12. The data in this figure is for 512 particles and was averaged over 6 runs with a measurement time of  $3 \times 10^6$  md steps. Notice that there is good agreement between calculating the specific heat by taking a derivative of the energy with respect to temperature (see eq. (13)) and by using fluctuations (see eq. (15)). This implies that the system has equilibrated within the basins that it visits in the energy landscape. We find similar agreement for shorter run times such as 200,000 and  $10^6$  md steps. At low temperatures the specific heat goes to  $3k_B$  as expected for Einstein oscillators while at high temperatures  $C_V$  approaches  $3k_B/2$  which corresponds to an ideal gas.

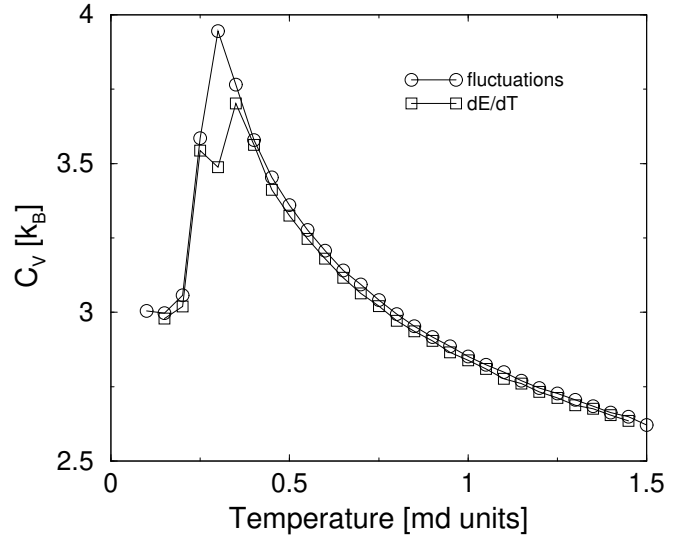


FIG. 12. Specific heat at constant volume as a function of temperature for binary mixture of 512 particles with a measuring time of  $3 \times 10^6$  md steps averaged over 6 runs.  $\rho_o = 0.6$  and  $\sigma_B/\sigma_A = 1.4$ . The specific heat is calculated from energy fluctuations and by taking the derivative of the energy with respect to temperature.

The peak in the specific heat occurs at  $T \approx 0.3$  which corresponds to  $\Gamma \approx 1.46$ . The temperature of the peak coincides with the mode coupling  $T_C = 0.303$  that we deduced from the intermediate scattering function data. Longer run times lead to a sharper peak in the specific heat as can be seen in Figure 13 which shows the specific heat for 512 particles for several different measuring times. The peaks would presumably be sharper if we had used a finer temperature scale. At high temperatures the agreement between the different times is very good. Perera and Harrowell [30] have found a specific heat peak in a two dimensional binary mixture of soft spheres. They argue that their peak is an equilibrium feature. However, in our case, at temperatures below the peak, the system has fallen out of equilibrium and has become trapped in

a basin in the energy landscape. We shall see this later by examining the energy of the inherent structures (potential energy minima) as a function of temperature.

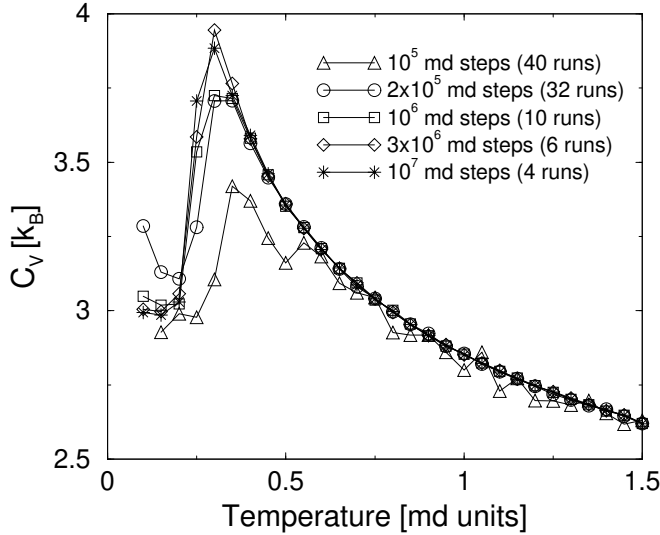


FIG. 13. Specific heat at constant volume as a function of temperature for binary mixture of 512 particles with measuring times of  $10^5$ ,  $2 \times 10^5$ ,  $10^6$ ,  $3 \times 10^6$ , and  $10^7$  md time steps. The number of runs averaged over is indicated in the legend. The specific heat is calculated from energy fluctuations.  $\rho_o = 0.6$  and  $\sigma_B/\sigma_A = 1.4$ .

The specific heat  $C_P$  of experimental systems at constant pressure exhibits a downward step at the glass transition during cooling and a peak at slightly higher temperatures upon heating [31]. As can be seen in Figure 14, in our warming up simulations, which are done at constant volume, the specific heat peak sharpens and moves toward higher temperatures compared to the cooling runs. This is consistent with what is seen in experiments. The hysteresis is consistent with the system falling out of equilibrium and getting stuck in a basin of the energy landscape.

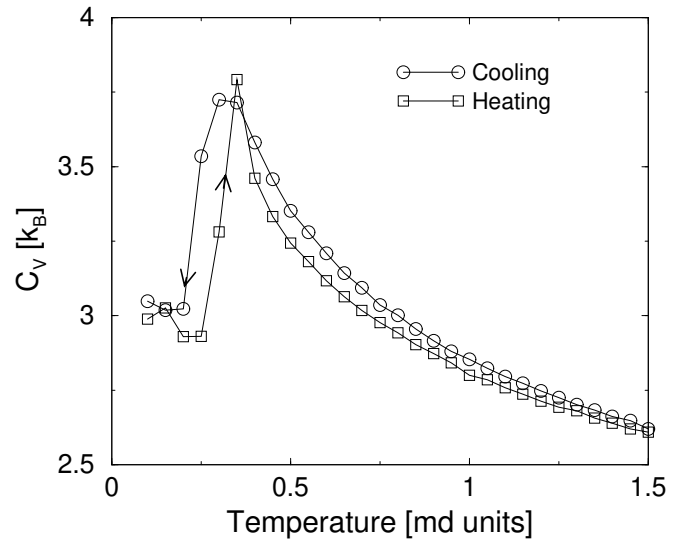


FIG. 14. Specific heat at constant volume during heating and cooling a binary mixture of 512 particles with a measuring time of  $10^6$  md time steps averaged over 10 runs.  $\rho_o = 0.6$  and  $\sigma_B/\sigma_A = 1.4$ .

As we mentioned in the introduction, some have suggested that the glass transition has an underlying second order phase transition [13–18]. Unlike typical second order phase transitions, there is no experimental evidence that the specific heat diverges at the glass transition. This is consistent with our simulations. In simulations one looks for a divergence by examining whether the quantity increases systematically with system size. In Figure 15 we plot  $C_V$  for systems with 216 and 512 particles. As one can see, the specific heat does not exhibit any size dependence.

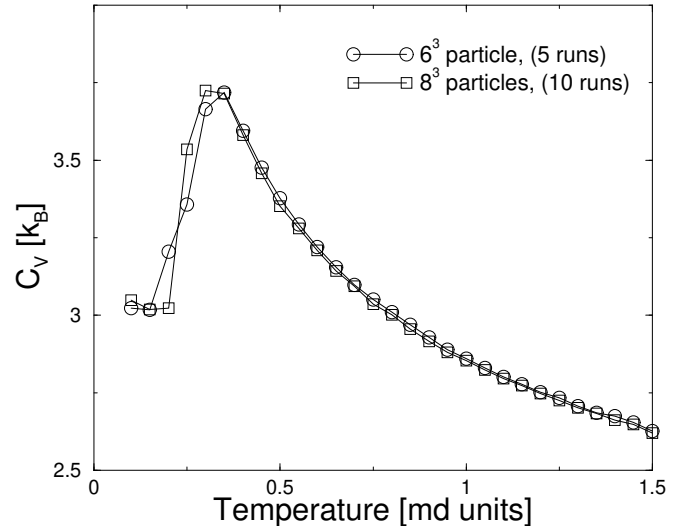


FIG. 15. Specific heat during cooling for binary mixtures of 216 and 512 particles. The measuring time was  $10^6$  md time steps. The specific heat was calculated from fluctuations and averaged over the number of runs indicated in the legend. Note the lack of size dependence.  $\rho_o = 0.6$  and  $\sigma_B/\sigma_A = 1.4$ .

## 2. Specific Heat Versus Density

In Figure 16 we show the specific heat as a function of density. As the density increases, the specific heat rises to a peak at  $\rho_o^{\text{peak}} = 0.8$ . This corresponds to  $\Gamma = 1.44$  which is in good agreement with the  $\Gamma$  value of 1.46 that we found for the specific heat peak when we varied the temperature. Going to higher densities corresponds to going to lower temperatures. At densities higher than 0.8, the system falls out of equilibrium.

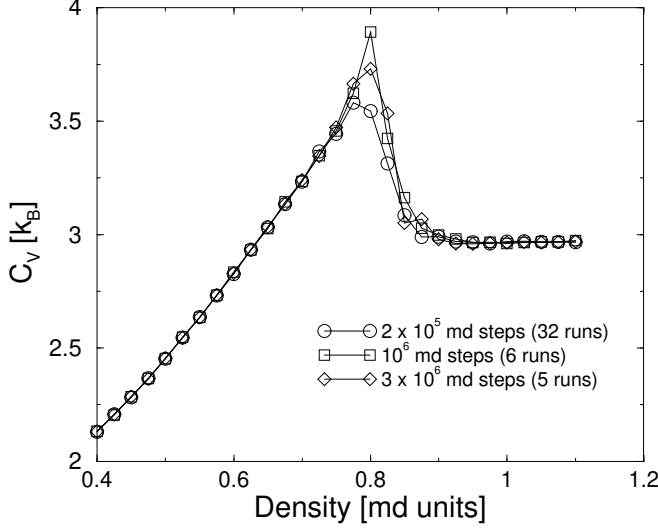


FIG. 16. Specific heat versus density for a binary mixture of 512 particles with  $T = 1$ . The measuring times were  $2 \times 10^5$ ,  $10^6$  and  $3 \times 10^6$  md time steps. The specific heat was calculated from fluctuations and averaged over the number of runs indicated in the legend.  $\rho_o = 0.6$  and  $\sigma_B/\sigma_A = 1.4$ .

## D. Linear Generalized Compressibility

As we mentioned in the introduction, the generalized compressibilities are thermodynamic probes that are a function of the microscopic structure of the system. They are solely a function of the positions of the particles and do not depend on their histories. So one could take snapshots of the configurations of the particles at different instances, scramble the order of the snapshots, and still be able to calculate the generalized compressibilities. Averaging over these snapshots corresponds to ensemble averaging. In this sense the generalized compressibilities are thermodynamic quantities which can be calculated solely from the microstates of the system and do not depend on the system's dynamics or kinetics.

### 1. Absolute Value of Positions versus Temperature

We will first discuss the linear generalized compressibility calculated from the absolute values of the positions

using eqs. (10) and (11).

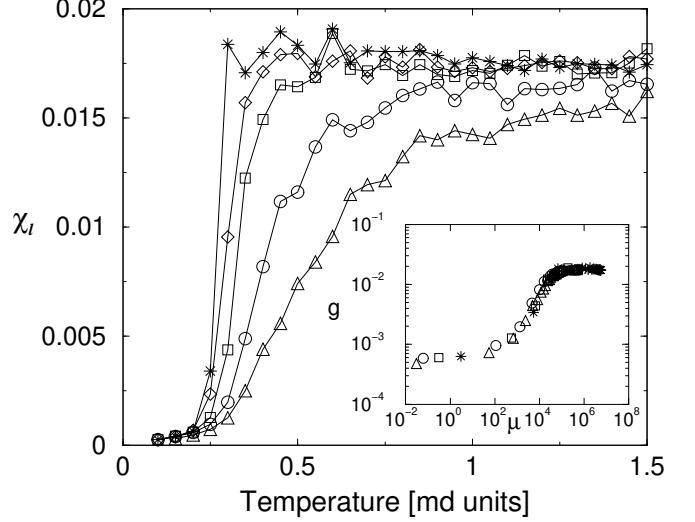


FIG. 17. Linear generalized compressibility as a function of temperature for different measuring times  $t_M$ :  $10^5$  ( $\triangle$ , 40 runs),  $2 \times 10^5$  ( $\circ$ , 32 runs),  $10^6$  ( $\square$ , 10 runs),  $3 \times 10^6$  ( $\diamond$ , 6 runs) and  $10^7$  ( $*$ , 4 runs) md steps. System size is 512 particles.  $\rho_o = 0.6$  and  $\sigma_B/\sigma_A = 1.4$ .  $\chi_l$  is calculated using the absolute value of the particles' positions. Inset:  $T > T_o$  subset of the same data scaled as described in text.

Figure 17 shows the linear generalized compressibility as a function of temperature for different run times. The compressibility at high temperatures is independent of  $T$  and about an order of magnitude larger than that of the crystal-forming single component fluid. In the vicinity of the glass transition  $\chi_l$  drops. Notice that as the measuring time  $t_M$  increases, the temperature of the drop decreases and becomes more abrupt. The measuring time can be thought of as the number of snapshots at a single temperature that we use to calculate the compressibility. The linear compressibility is proportional to the width of the distribution of  $\rho_\phi$ , so the drop in  $\chi_l$  corresponds to the sudden narrowing of the distribution  $P(\rho_\phi)$ . If we regard  $\rho_\phi$  as a generalized center of mass, then the drop in  $\chi_l$  signals the sudden arrest in the fluctuations of the generalized center of mass. In other words, at the glass transition the motion of the particles is largely frozen and hence, the generalized center of mass does not move around much. This is consistent with recent observations of the colloidal glass transition in which the size of the clusters of “fast” particles drops dramatically at the glass transition [21].

Notice that at longer measuring times, the temperature  $T_{\text{drop}}$  at which the generalized linear compressibility drops is roughly at the mode coupling temperature  $T_C = 0.303$ . Let us define  $T_{\text{drop}}$  as the temperature at which  $\chi_l$  has dropped halfway down. For  $10^6$  md steps,  $T_{\text{drop}} \approx 0.33$ ; for  $3 \times 10^6$  md steps,  $T_{\text{drop}} \approx 0.30$ ; and for  $10^7$  md steps,  $T_{\text{drop}} \approx 0.27$ . Thus we are able to stay in equilibrium down to the mode coupling temperature for

our longer runs. This is what we would expect when we compare these run times, which are longer than 1 million time steps, to the  $\alpha$  relaxation time  $\tau$  which is slightly less than 1 million time steps at  $T = 0.29$  which is just below  $T_C$ .

This behavior exhibited by  $\chi_l$  can be quantified using a scaling ansatz:  $\chi_l(t_M, T) = g(\mu = t_M/\tau(T))$ , where the characteristic time has the Vogel–Fulcher form  $\tau(T) = \exp(A/(T - T_o))$ . The inset of Figure 17 shows that the data collapse onto a single curve with  $A = 0.75$ ,  $T_o = 0.15$ . (The data could not be fitted using  $\tau(T) = A(T - T_o)^\gamma$  as suggested by simple mode coupling theories [3].) Notice that  $T_o$  lies below the Vogel–Fulcher temperature  $T_{VF} = 0.21$  and the MCT critical temperature  $T_C = 0.303$  deduced by fitting temperature dependence of the relaxation times. This scaling suggests that  $\chi_l$  becomes a step function for infinite  $t_M$  and that the drop in the compressibility would become a discontinuity at infinitely long times. This abrupt drop is consistent with a sudden arrest of the motion of the particles in the liquid which is the kinetic view of the glass transition. The abrupt drop also appears to be in agreement with Mezard and Parisi’s proposal that the glass transition is a first order phase transition with a jump in the specific heat [19,12]. Indeed the temperature at which  $\chi_l$  drops agrees with the temperature of the peak in the specific heat shown in Figure 13. This provides an independent check of the glass transition temperature. However, the drop in  $\chi_l$  and the specific heat peak are due to the system falling out of equilibrium, and therefore we cannot really tell if there is a true thermodynamic transition.

One way to see that the system is falling out of equilibrium is to plot the inherent structure energy per particle [32,33,9]. An inherent structure is a particular system configuration whose energy corresponds to the minimum of a basin in the energy landscape. The energy landscape is a  $3N$  dimensional surface defined by the potential energy of the system which is a function of the particles’ coordinates. During each run we saved the last particle configuration found at each temperature. Each configuration lies somewhere in a basin and we used the method of conjugate gradients [34] to find the inherent structure energy of that basin. The result is shown in Figure 18. At high temperatures the inherent structure energy  $e_{IS}$  per particle is flat as a function of temperature. As the system is cooled,  $e_{IS}$  decreases rather steeply [9]. The inherent structure energy flattens off at low temperatures where the system has fallen out of equilibrium and has become stuck in one basin. For each measuring time the temperature below which the generalized linear compressibility drops corresponds to the temperature below which the inherent structure energy flattens off at low temperatures. Thus the temperature of the drop in  $\chi_l$  and the peak in the specific heat corresponds to the temperature below which the system falls out of equilibrium and ceases to explore deeper basins of the energy land-

scape.

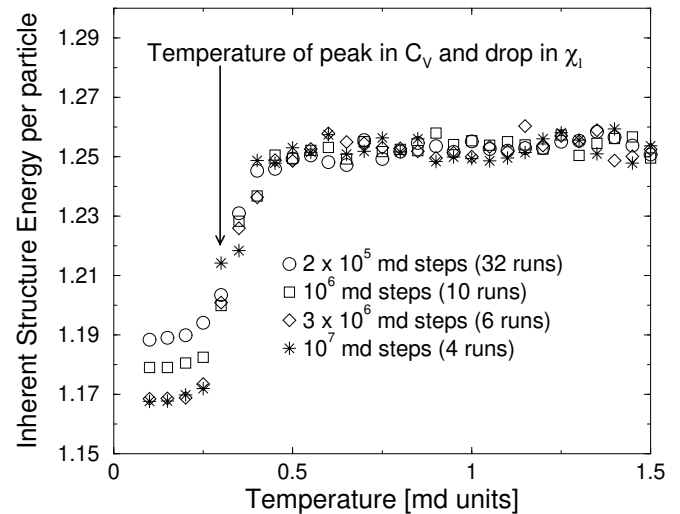


FIG. 18. Inherent structure energy per particle as a function of temperature for a system of 512 particles at different measuring times. The number of runs indicates the number of configurations used per temperature to calculate the inherent structure energy. Other parameters are the same as in Figure 17.

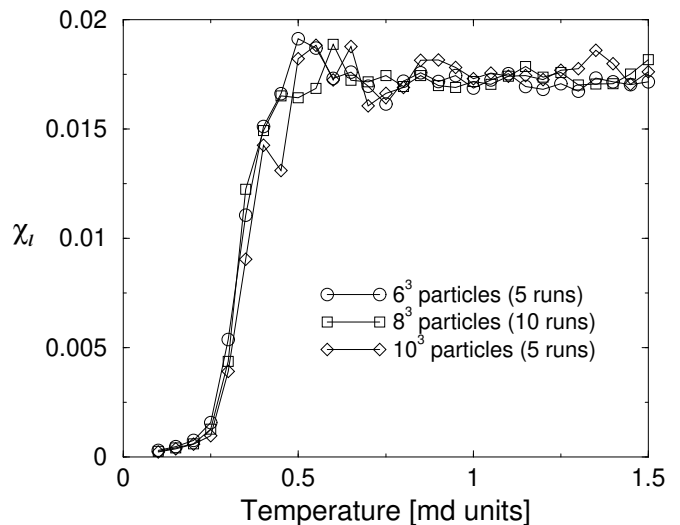


FIG. 19. Linear compressibility as a function of temperature for different system sizes: 216, 512 and 1000 particles. The measuring time was  $10^6$  md steps in all cases. Other parameters are the same as in Figure 17.

The behavior of the linear generalized compressibility seen in Figure 17 is similar to that seen in measurements of the real part of the frequency dependent dielectric function  $\epsilon'(\omega)$  [18]. In that case as the frequency decreased, the temperature of the peak in  $\epsilon'(\omega)$  decreased and the drop in  $\epsilon'(\omega)$  below the peak became more abrupt. By extrapolating their data to  $\omega = 0$ , Menon and Nagel [18] argued that  $\epsilon'(\omega = 0)$  should di-

verge at the glass transition, signaling a second order phase transition. We have looked for evidence of this divergence by examining samples of different sizes to see if the linear generalized compressibility increased systematically with system size. As shown in Figure 19 we find no size dependence and no indication of a diverging linear generalized compressibility.

So far we have shown the results of cooling the system. In order to look for hysteretic behavior we have done runs in which we heat a system of 512 particles by starting at our lowest temperature  $T = 0.1$  with a configuration obtained by cooling the system. We then increased the temperature in steps of  $\Delta T = 0.05$ . As before we equilibrate at each temperature for  $10^4$  time steps and then measure quantities for an additional  $10^6$  time steps. Our results are shown in Figure 20. Notice the slight hysteresis with the rise in  $\chi_l$  upon warming being at a slightly higher temperature than the drop in  $\chi_l$  upon cooling. This hysteresis is consistent with the kinetic arrest of motion and with the hysteresis found for the specific heat in Figure 14.

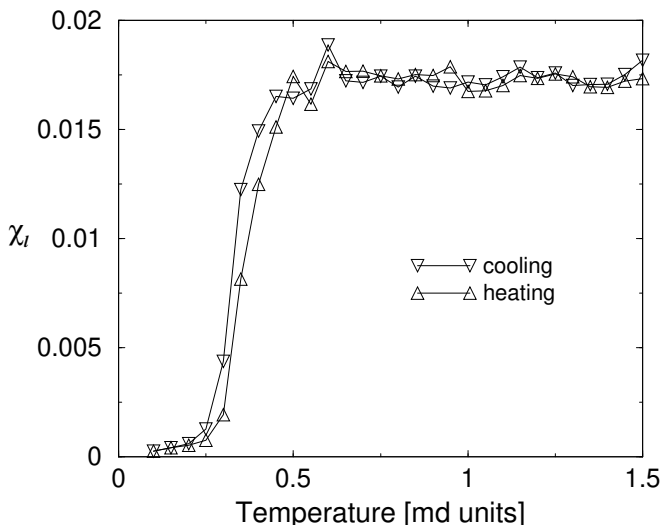


FIG. 20. Linear generalized compressibility as a function of temperature for a binary mixture of 512 particles upon cooling and heating. The measuring time was  $10^6$  md steps in both cases. The data was averaged over 10 runs. Other parameters are the same as in Figure 17.

## 2. Cosine of Positions versus Temperature

We now consider calculating the linear generalized compressibility from the cosine transform of the density using eqs. (10) and (12). So if we apply a cosine potential along, say the  $\mu = x$  direction, then

$$\rho_\phi = \sum_i \cos(k_x x_i) \quad (24)$$

where the wavevector  $k_x = 2\pi n/L$  with  $n = 1, 2, \dots$ . The wavevectors are compatible with the periodic bound-

ary conditions of our simulations. Since the system is isotropic, we average  $\chi_l$  over the  $x$ ,  $y$ , and  $z$  directions. The resulting linear generalized compressibility is qualitatively similar in its temperature dependence to the linear compressibility calculated using the absolute values of the particles' positions (eq. (11)). Figure 21 shows the linear generalized compressibility versus temperature for various values of the wavevector. The data is for a binary mixture of 512 particles with a measuring time of  $10^6$  md steps and averaged over 10 runs.

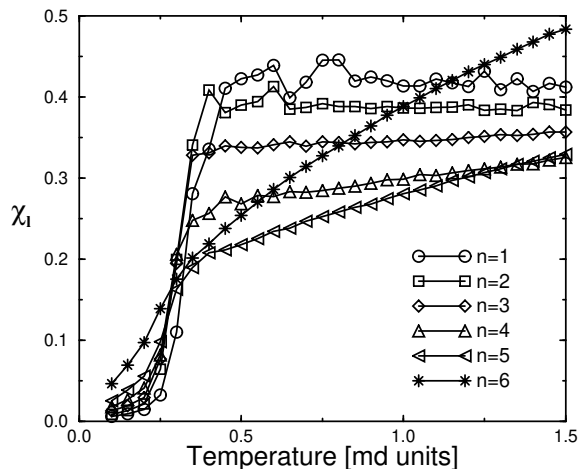


FIG. 21. Linear generalized compressibility as a function of temperature for a binary mixture of 512 particles for different values of the wavevector  $k = 2\pi n/L$ . The measuring time was  $10^6$  md steps in all cases. The data was averaged over 10 runs. The susceptibility was calculated using eqs. (10) and (12). Other parameters are the same as in Figure 17.

Just as for the absolute value case, we find that as we increase the measuring time, the drop in the linear generalized compressibility calculated using a cosine potential becomes sharper at the glass transition. This is shown in Figure 22 which shows  $\chi_l$  as a function of temperature for measuring times of  $2 \times 10^5$ ,  $10^6$ , and  $3 \times 10^6$  md steps with  $k = 2\pi/L$ , i.e.,  $n = 1$ .

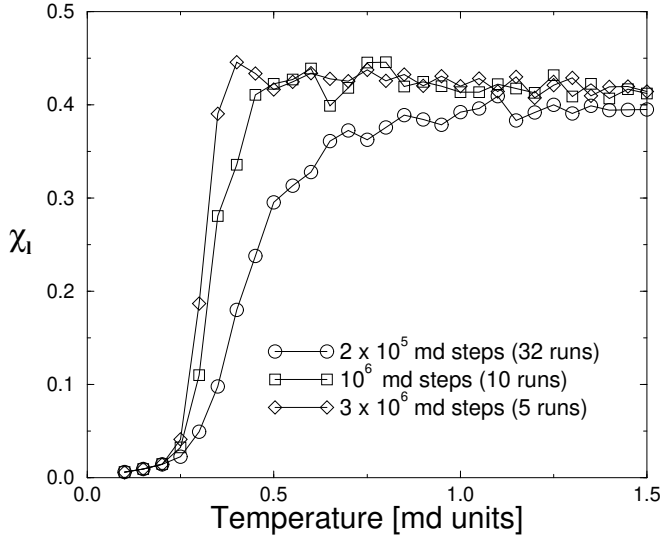


FIG. 22. Linear generalized compressibility as a function of temperature for a binary mixture of 512 particles for different values of the measuring time. The measuring times are  $2 \times 10^5$ ,  $10^6$ , and  $3 \times 10^6$  md steps. The data was averaged over the number of runs indicated in the legend. The susceptibility was calculated using eqs. (10) and (12). The wavevector  $k = 2\pi/L$ , i.e.,  $n = 1$ . Other parameters are the same as in Figure 21.

Figure 23 shows the linear generalized susceptibility versus the wavevector  $k$  in units of  $2\pi/L$  for various temperatures. Note that the dependence is nonmonotonic.

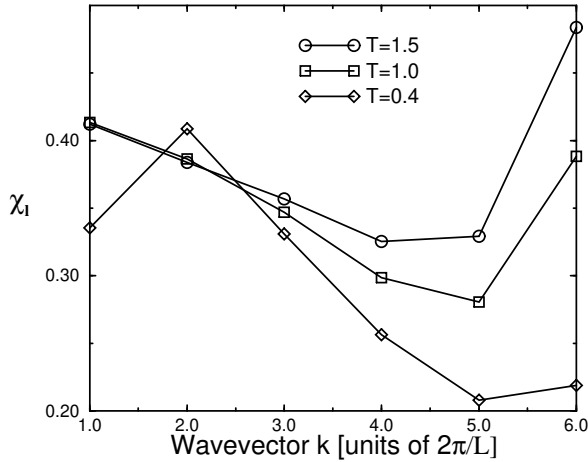


FIG. 23. Linear generalized compressibility as a function of wavevector for a binary mixture of 512 particles for different values of the temperature. The temperature is measured in md units. The measuring time was  $10^6$  md steps in all cases. The data was averaged over 10 runs. The susceptibility was calculated using eqs. (10) and (12). Other parameters are the same as in Figure 21.

### 3. Generalized Linear Compressibility Versus Density

In Figure 24 we plot the generalized linear compressibility versus density calculated from the absolute value of the positions of the particles. In Figure 25 we plot the generalized linear compressibility versus density calculated from the cosine of the particles' positions. In both cases we see that  $\chi_l$  drops with increasing density. The drop becomes more abrupt as the measuring time increases. This drop is similar to what we see when we cool the system at fixed density. The density ( $\rho \approx 0.8$ ,  $\Gamma \approx 1.44$ ) at which the drop occurs agrees with the density at which there is a peak in the specific heat as shown in Fig. 16.

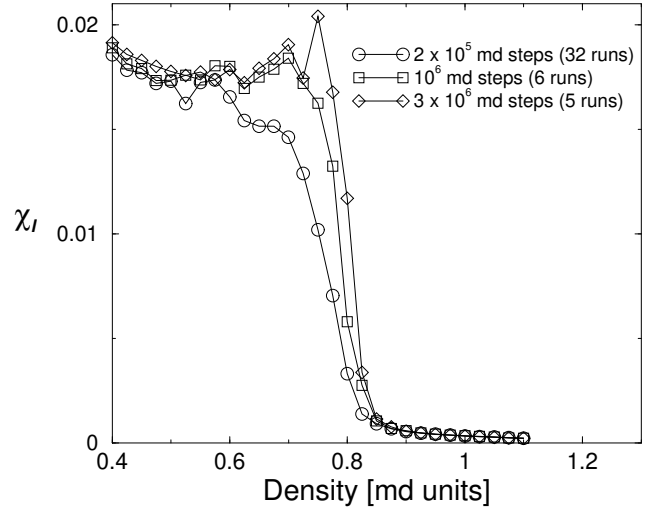


FIG. 24. Generalized linear compressibility as a function of density for a binary mixture of 512 particles at  $T = 1$ . The measurement times are  $2 \times 10^5$ ,  $10^6$  and  $3 \times 10^6$  md steps.  $\sigma_B/\sigma_A = 1.4$ . Data was averaged over the number of runs indicated in the legend.  $\chi_l$  is calculated using the absolute value of the particles' positions.

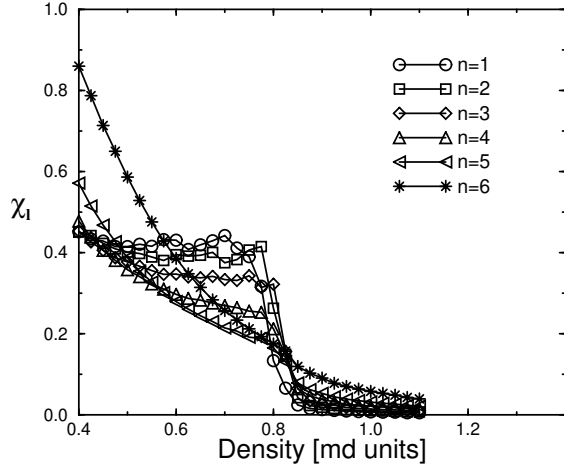


FIG. 25. Generalized linear compressibility as a function of density for a binary mixture of 512 particles at  $T = 1$ . The different values of  $n$  correspond to different values of the wavevector  $k = 2\pi n/L$ . The measurement time is  $10^6$  md steps in all cases.  $\sigma_B/\sigma_A = 1.4$ . Data was averaged over 6 runs. The susceptibility was calculated from the cosine of the particles' positions using eqs. (10) and (12). Other parameters are the same as in Figure 21.

#### 4. Absolute Value of Positions versus Temperature in a Slab Geometry

So far we have considered systems with a fixed number of particles, but as we mentioned earlier in section IIID, we can generalize our results to the grand canonical ensemble with the number  $N$  of particles allowed to vary. We have examined the generalized linear compressibility  $\chi_l$  from the absolute value of the particle positions using equations (10) and (11) for a slab of our system. In other words we have divided a system of  $8^3$  particles into 8 slabs perpendicular to the  $x$  axis of equal thickness. The number of particles in any given slab is not fixed. However, in eq. (10) we set the average number of particles  $N$  in each slab equal to the total number of particles in the system divided by the number of layers, i.e.,  $N = 8^3/8 = 64$ . Such a slab geometry mimicks experiments on colloidal suspensions of binary mixtures in which the focal plane of the camera can essentially see only one monolayer of polystyrene balls [35]. In figure 26 we show the generalized linear compressibility for a slab for two different times. Again we see that the drop is sharper as the measurement time becomes longer. Thus allowing for fluctuations in the number of particles does not change the qualitative behavior of  $\chi_l$  at the glass transition. Comparing Figures 17 and 26, we see that the temperature of the drop for the slab and the bulk agree. We also notice that the drop is sharper for the bulk where presumably the greater number of particles results in better statistical averaging.

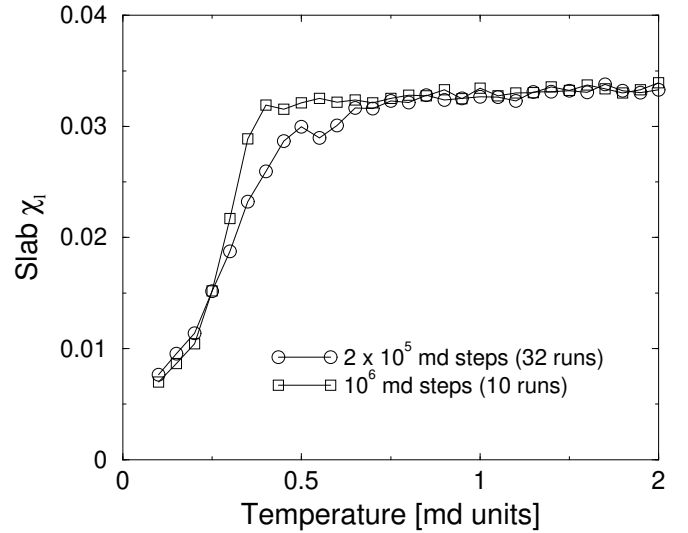


FIG. 26. Linear generalized compressibility as a function of temperature for a monolayer slab in a binary mixture of 512 particles for different values of the measuring time. The measuring times are  $2 \times 10^5$  and  $10^6$  md steps. The data was averaged over the number of runs indicated in the legend. The susceptibility was calculated using eqs. (10) and (11). Other parameters are the same as in Figure 17.

#### 5. Absolute Value of Positions versus Density in a Slab Geometry

Since experiments on colloidal suspensions usually vary the density rather than the temperature, we have done simulations where we set the temperature  $T = 1$  and vary the density. Again we divide our system of  $N = 8^3 = 512$  particles into 8 slabs and measure  $\chi_l$  in one of those slabs. The results are shown in Figure 27.

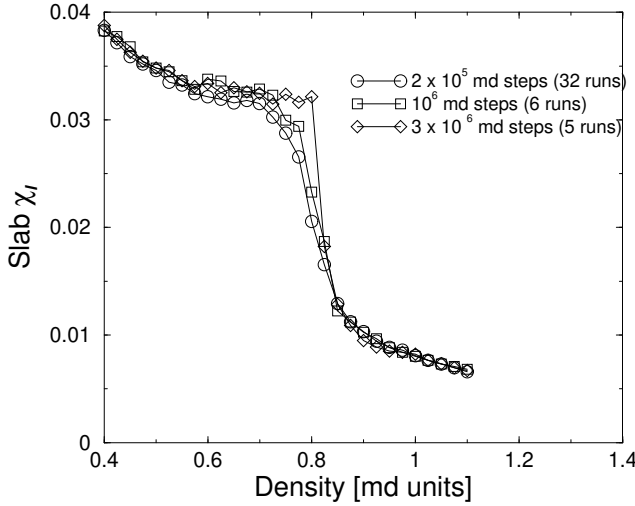


FIG. 27. Linear generalized compressibility as a function of density for a monolayer slab in a binary mixture of 512 particles for different values of the measuring time. The measuring times are  $2 \times 10^5$ ,  $10^6$  and  $3 \times 10^6$  md steps. The data was averaged over the number of runs indicated in the legend. The susceptibility was calculated using eqs. (10) and (11). Other parameters are the same as in Figure 17.

As one can see from the figure,  $\chi_l$  drops as the density is increased and the drop becomes more abrupt as the measuring time lengthens. Comparing Figures 24, 25 and 27, we see that the drop occurs at the same density ( $\rho \approx 0.8$ ) as in the bulk.

### E. Ordinary Isothermal Compressibility versus Temperature

As we discussed in section IIID, in the grand canonical ensemble the ordinary isothermal compressibility  $\kappa_T$  is proportional to the linear generalized compressibility if we choose a uniform potential. In our simulations we fix the volume and the number of particles  $N$  so the system has no real compressibility. However we can calculate the isothermal compressibility by monitoring the fluctuations in the number of particles in a subset of our sample. Let us define a dimensionless ordinary isothermal compressibility  $K_T$  by

$$\kappa_T = \frac{1}{\rho k_B T} K_T \quad (25)$$

where

$$K_T = \frac{\langle N^2 \rangle - \langle N \rangle^2}{\langle N \rangle} \quad (26)$$

In order to calculate  $K_T$ , we have monitored a subvolume that had 128 particles on average out of a total of 512 particles. Essentially we drew an imaginary boundary in the middle of our system that enclosed 25% of the total volume and counted the number of particles in this

subvolume as a function of time. By monitoring the fluctuations in the number of particles in this subvolume, we could calculate  $K_T$ . The results are shown in Figure 28 where  $K_T$  is plotted versus temperature. We see that it has the same basic shape as the linear generalized compressibility with a drop at the same temperature as  $\chi_l$ . As with  $\chi_l$ , the drop becomes sharper with increasing measuring time.

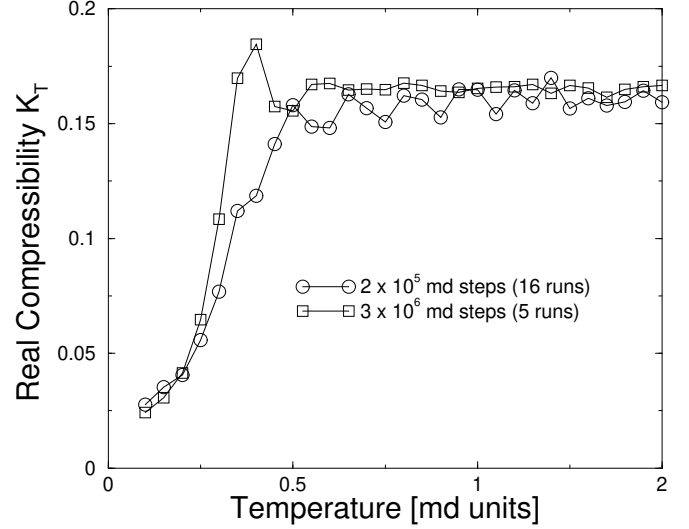


FIG. 28. Dimensionless ordinary isothermal compressibility  $K_T$  as a function of temperature for a subset of a system of 512 particles for different values of the measuring time. On average the subset had 128 particles in it. The measuring times are  $2 \times 10^5$  and  $3 \times 10^6$  md steps. The data was averaged over the number of runs indicated in the legend. The dimensionless compressibility was calculated using eq. (26). Other parameters are the same as in Figure 17.

### F. Nonlinear Generalized Compressibility

We now turn to the case of the nonlinear generalized compressibility  $\chi_{nl}$  given by eq. (10). We are motivated by the case of spin glasses where the nonlinear magnetic compressibility diverges at the spin glass transition while the linear compressibility only has a cusp [36,37]. There have been a few studies of nonlinear response functions in structural glasses [17,38], but these have not found any divergences. Our results are consistent with this conclusion. In particular we find that the nonlinear generalized compressibility is zero above and below the glass transition temperature, though it does show a glitch at the glass transition temperature. There is no systematic increase with system size, indicating the absence of a divergence. Because  $\chi_{nl}$  is sensitive to the tails of the distribution of  $\rho_\phi$ , one must be careful to obtain a good ensemble average in the liquid above the glass transition temperature. We have done this by doing 32 runs, each involving 200,000 time steps, with different initial condi-



tions, stringing them together as though they were one long run and then taking the appropriate averages. In some sense this approach mixes molecular dynamics and Monte Carlo; the simulation follows the equations of motion for a given amount of time and then “jumps” to another configuration which again evolves according to the molecular dynamics equations until the next jump. We call this approach “global averaging.” It produces a better ensemble average of  $\langle \rho_\phi^2 \rangle^2$  which enters into  $\chi_{nl}$  in eq. (7). The result is shown in Figure 29 which was calculated from the absolute values of the particles’ positions using eqs. (10) and (11).

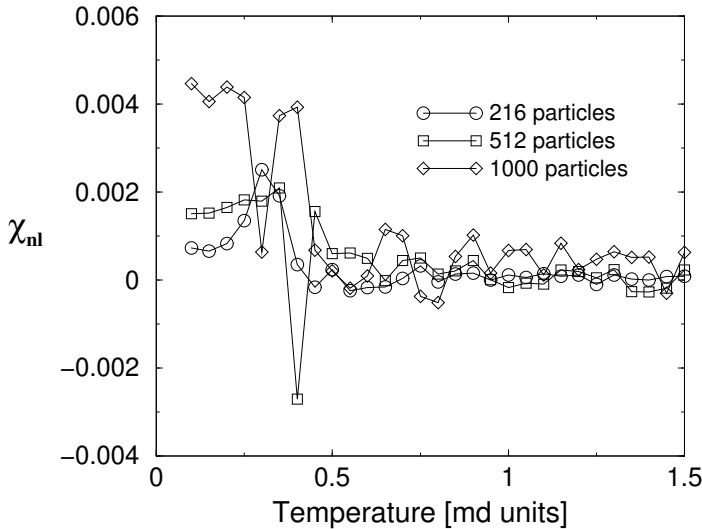


FIG. 29. Nonlinear generalized compressibility as a function of temperature for binary mixtures. The data for 216 particles is from  $3.2 \times 10^6$  md steps obtained by stringing together 16 runs, each of which involved  $2 \times 10^5$  md steps. The data for 512 and 1000 particles is from  $6.4 \times 10^6$  md steps obtained by stringing together 32 runs of  $2 \times 10^5$  md steps.  $\rho_o = 0.6$  and  $\sigma_B/\sigma_A = 1.4$ .

$\chi_{nl}$  also took longer to equilibrate than  $\chi_l$ . By plotting  $\chi_{nl}$  versus run time, we found that one had to run at least  $10^6$  time steps before  $\chi_{nl}$  appeared to saturate (see Figure 30).

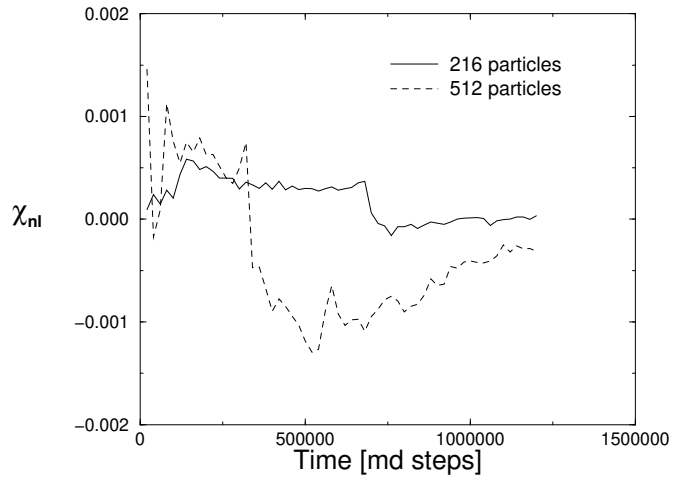


FIG. 30. Nonlinear generalized compressibility as a function of time for binary mixtures of 216 and 512 particles at  $T = 1$ . The data shown for each system size is for a single run and a running average is kept.  $\chi_{nl}$  is calculated using eqs. (10) and (11).  $\rho_o = 0.6$  and  $\sigma_B/\sigma_A = 1.4$ .

## VI. RELATION BETWEEN $\chi_L$ AND $S(k)$

By definition, the static structure factor  $S(\vec{k}) = (1/N)\langle \rho_{\vec{k}} \rho_{-\vec{k}} \rangle$  where  $N$  is the number of particles and  $\rho_{\vec{k}} = \sum_{i=1}^N \exp(-i\vec{k} \cdot \vec{r}_i)$  is the Fourier transform of the local density  $\rho(\vec{r})$ . When the system has translational invariance, we can relate the linear generalized compressibility  $\chi_l$  to the structure factor  $S(k)$  which is measured in experiments such as neutron scattering.  $S(k)$  is also used as an input for mode coupling theories [3] and it is generally assumed that  $S(k)$  does not show any essential variations near the glass transition as the temperature or density is varied. As we shall see, our calculation agrees with this.

To relate  $S(k)$  to  $\chi_l$ , we first note that  $S(k)$  is the Fourier transform of the static density-density autocorrelation function  $G(\vec{r})$ , i.e.,  $S(\vec{k}) = \int \exp(-i\vec{k} \cdot \vec{r}) G(\vec{r}) d^3r$ , where  $G(\vec{r}) = (1/N) \int \langle \rho(\vec{r}' + \vec{r}) \rho(\vec{r}') \rangle d^3r'$ . In the supercooled liquid above the glass transition, the system has translational invariance, and we can write

$$\langle \rho(\vec{r}) \rho(\vec{r}') \rangle = \frac{1}{V} g(\vec{r} - \vec{r}') \quad (27)$$

where  $V$  is volume and  $g$  is a function of the difference  $(\vec{r} - \vec{r}')$ . In this case  $G(\vec{r}) = g(\vec{r})/N$ . In  $\chi_l$  we meet

$$\langle \rho_\phi^2 \rangle = \int d^3r d^3r' \phi(\vec{r}) \phi(\vec{r}') \langle \rho(\vec{r}) \rho(\vec{r}') \rangle \quad (28)$$

If there is translational invariance,

$$\begin{aligned} \langle \rho_\phi^2 \rangle &= \frac{1}{V} \int d^3r d^3r' \phi(\vec{r}) \phi(\vec{r}') g(\vec{r} - \vec{r}') \\ &= \frac{1}{V} \int \frac{d^3k}{(2\pi)^3} \phi(\vec{k}) \phi(-\vec{k}) g(-\vec{k}) \end{aligned}$$

$$= \rho_o \int \frac{d^3k}{(2\pi)^3} |\phi(\vec{k})|^2 S(\vec{k}) \quad (29)$$

where  $\phi(\vec{k})$  is the Fourier transform of  $\phi(\vec{r})$ . Converting the integral  $V \int d^3k/(2\pi)^3$  to a sum  $\sum_{\vec{k}}$  and using eq. (10), we obtain

$$\chi_l = \frac{6}{N} \left[ \frac{N}{V^2} \sum_{\vec{k}} (|\phi(\vec{k})|^2 S(\vec{k})) - \langle \rho_\phi \rangle^2 \right] \quad (30)$$

As an example, let us choose  $\phi(\vec{r}) = \cos(k_x x)$  with the proviso that  $k_x \neq 0$ . (When  $\vec{k} = 0$ ,  $\chi_l = 0$  since the potential is uniform and there are no fluctuations allowed with fixed  $N$  and  $V$ .) With this choice of  $\phi(\vec{r})$ ,  $\rho_\phi = \sum_i \cos(k_x x_i)$ . Then one can show by explicitly calculating  $\phi(\vec{k})$  and by using eqs. (29) and (30) that

$$\chi_l(\vec{k}) = 3S(\vec{k}) - \frac{6}{N} [\text{Re} \langle \rho_{\vec{k}} \rangle]^2 \quad (31)$$

where translational invariance allows us to write

$$S(\vec{k}) = (2/N) \langle \rho_\phi^2 \rangle \\ = (2/N) \sum_{ij} [\langle \cos(k_x x_i) \cos(k_x x_j) \rangle] \quad (32)$$

$$(33)$$

Note that the value of  $k$  that we use to probe the glass transition is typically of order  $k_L \equiv 2\pi/L$  which is much smaller than the value of  $k_{\text{peak}}$  at which the first peak in  $S(k)$  appears.  $k_{\text{peak}} \sim 2\pi/\sigma_A \gg k_L$  where  $\sigma_A$  is the diameter of type A spheres in the binary mixture.

We have numerically calculated  $[S(k)]_{\text{run}}$  for our binary mixture using equation (32) with  $\phi(\vec{r}) = \cos(k_\mu r_\mu)$ . (No sum over repeated indices.  $\mu = x, y$ , or  $z$ .)  $[\dots]_{\text{run}}$  is an average over all the runs and over  $\vec{k}$  being parallel to  $x$ ,  $y$ , and  $z$ . The result is shown in Figure 31 and one can see that  $[S(k)]_{\text{run}}$  does not vary much through the glass transition which is consistent with what is assumed in mode coupling theory. The figure also shows  $[\text{Re} \langle \rho_k \rangle]_{\text{run}}$  where  $\langle \dots \rangle$  is a thermal average over a single run. If  $[S(k)]_{\text{run}}$  and  $[\text{Re} \langle \rho_k \rangle]_{\text{run}}$  do not vary much through the glass transition, how can the difference between the two terms in (31) decrease and produce a drop in  $\chi_l$ ? To answer this, note that there are two inequivalent ways in which one can calculate  $\chi_l$ . So far we have calculated  $\chi_l$  for each run and then averaged over the different runs. This approach is what we used in Figs. 17–20 and results in a sharp drop in the linear generalized compressibility at the glass transition. Let us call this a run-by-run average for which we can write:

$$\chi_l = \frac{6}{N} [\langle \rho_\phi^2 \rangle - \langle \rho_\phi \rangle^2]_{\text{run}} \quad (34)$$

The drop in  $\chi_l$  comes about because the width of the distribution of  $\text{Re}(\rho_k)$  becomes much smaller below the

transition. At low temperatures structural arrest hinders the exploration of phase space and reduces the fluctuations in  $\text{Re}(\rho_k)$ .

The other way to calculate the generalized linear compressibility is global averaging in which in which we string together a series of separate runs, treat it as one giant run, and then do the averaging required to calculate the generalized linear compressibility  $\chi_l^{\text{global}}$ .

$$\chi_l^{\text{global}} = \frac{6}{N} \left\{ [\langle \rho_\phi^2 \rangle]_{\text{run}} - ([\langle \rho_\phi \rangle]_{\text{run}})^2 \right\} \quad (35)$$

Careful inspection of eqs. (34) and (35) reveals that the difference is in whether we square the thermal average  $\langle \rho_\phi \rangle$  and then average over runs to obtain  $[\langle \rho_\phi \rangle^2]_{\text{run}}$  in  $\chi_l$ , or average  $\langle \rho_\phi \rangle$  over runs and then square it to obtain  $([\langle \rho_\phi \rangle]_{\text{run}})^2$  in  $\chi_l^{\text{global}}$ . If we now return to Figure 31 and take the difference of  $[S(k)]_{\text{run}}$  and  $[\text{Re} \langle \rho_k \rangle]_{\text{run}}^2$ , we obtain the global average:

$$\chi_l^{\text{global}} = 3[S(k)]_{\text{run}} - \frac{6}{N} [\text{Re} \langle \rho_k \rangle]_{\text{run}}^2 \quad (36)$$

The result of both types of averaging is shown in Figures 31 and 32. Notice that  $\chi_l^{\text{global}}$  does not exhibit a drop with decreasing temperature while  $\chi_l$  does. To understand why there is no drop in  $\chi_l^{\text{global}}$ , note that by combining several different runs, very different configurations are sampled which produces much larger fluctuations in the generalized center of mass at low temperatures compared to  $\chi_l$ . As a result  $\chi_l^{\text{global}}$ , which is a measure of the size of these fluctuations, does not have an abrupt drop.

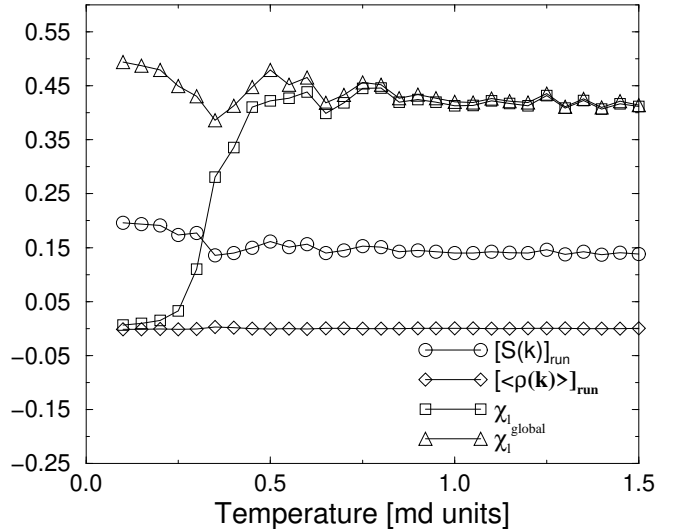


FIG. 31. Linear generalized compressibility  $\chi_l$ , static structure factor  $[S(k)]_{\text{run}}$ ,  $[\text{Re} \langle \rho_k \rangle]_{\text{run}}$ , linear generalized compressibility  $\chi_l$  averaged run by run, and the globally averaged linear generalized compressibility  $\chi_l^{\text{global}}$  versus temperature for a binary mixture of 512 particles. The measurement time was  $10^6$  md steps for each temperature. The data was averaged over 10 runs and over  $\vec{k} = (2\pi/L, 0, 0)$ ,  $\vec{k} = (0, 2\pi/L, 0)$ , and  $\vec{k} = (0, 0, 2\pi/L)$ .  $\rho_o = 0.6$  and  $\sigma_B/\sigma_A = 1.4$ .

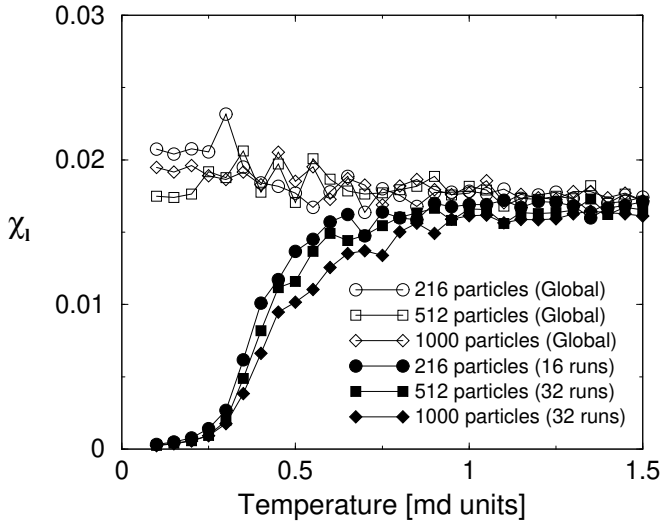


FIG. 32. Linear generalized compressibility as a function of temperature for binary mixtures of 216, 512 and 1000 particles. The filled symbols correspond to calculating  $\chi_l$  for each run with a measuring time of  $2 \times 10^5$  md steps and then averaging over the number of runs indicated in the legend, while the open symbols correspond to global averages (stringing all these runs together to get one big “run” for a given system size). So the global average for 216 particles uses  $3.2 \times 10^6$  md steps while for 512 and 1000 particles,  $6.4 \times 10^6$  md steps were used.  $\chi_l$  is calculated using eqs. (10) and (11).  $\rho_o = 0.6$  and  $\sigma_B/\sigma_A = 1.4$ .

## VII. SUMMARY

To summarize, we have introduced a new thermodynamic quantity which depends solely on the positions of the particles and not on their histories. This quantity drops abruptly at the glass transition which is at the mode coupling transition. This behavior is compatible with a kinetic arrest of motion, but not with an underlying second order phase transition. This generalized compressibility can be experimentally measured in several ways. It can be directly measured in colloidal experiments which monitor the positions of the particles. Measurements of the width of the distribution of  $\rho_q$ , the spatial Fourier transform of the density, would also yield the linear generalized compressibility.

We thank Andrea Liu for helpful discussions. This work was supported in part by DOE grant DE-FG03-00ER45843 as well as by CULAR funds provided by the University of California for the conduct of discretionary research by Los Alamos National Laboratory.

## VIII. APPENDIX: PARALLEL TEMPERING

In calculating the intermediate scattering function at a given temperature, we initialized the run using a configuration at that temperature generated by parallel tem-

pering. In this appendix we briefly describe the parallel tempering method.

We implement parallel tempering (PT) [39–42] by choosing the temperatures at which we wish to have measurements made. We then run molecular dynamics simulations in parallel at these temperatures using a temperature constraint algorithm [24] to keep the temperature of each simulation constant. At 100 time step intervals we attempt to switch the configurations of two neighboring temperatures using a Metropolis test which ensures that the energies of the configurations sampled at any given temperature have a Boltzmann distribution. Let  $\beta_1$  and  $\beta_2$  be two neighboring inverse temperatures, and let  $U_1$  and  $U_2$  be the corresponding potential energies of the configurations at these temperatures at a time step just before the possible swap. If  $\Delta = (\beta_1 - \beta_2)(U_2 - U_1)$ , then the switch is accepted with probability unity if  $\Delta \leq 0$  and with probability  $\exp(-\Delta)$  if  $\Delta > 0$ . The temperatures are chosen so that the acceptance ratio is between 30% and 75%. At the temperatures in the vicinity of the mode coupling  $T_C$ , the acceptance ratio was typically above 75% for  $L=6$  and above 60% for  $L=8$ . After a swap is accepted, the velocities of the particles in each configuration are rescaled to suit their new temperature. Each configuration is then evolved using molecular dynamics for another 100 time steps. Switching configurations allows a given simulation to do a random walk in temperature space in which it visits both low temperatures and high temperatures. This helps to prevent a simulation from becoming trapped in a valley of the energy landscape at low temperatures. Typically we equilibrate for 2 million time steps and then do measurements for an additional 4 million time steps.

<sup>†</sup>Present address: Internap, Seattle, WA 98101.

- 
- [1] M. D. Ediger, C. A. Angell, and S. R. Nagel, *J. Phys. Chem* **100**, 13200 (1996), and references therein.
  - [2] J. T. Fourkas, D. Kivelson, U. Mohanty, and K. A. Nelson, *Supercooled Liquids: Advances and Novel Applications* (American Chemical Society, Washington, D. C., 1997).
  - [3] W. Götze and L. Sjögren, *Rep. Prog. Phys.* **55**, 241 (1992).
  - [4] C. Donati *et al.*, *Phys. Rev. Lett.* **80**, 2338 (1998).
  - [5] R. Yamamoto and A. Onuki, *Europhys. Lett.* **40**, 61 (1997).
  - [6] R. Yamamoto and A. Onuki, *J. Phys. Soc. (Japan)* **66**, 2545 (1997).
  - [7] U. Tracht *et al.*, *Phys. Rev. Lett.* **81**, 2727 (1998).
  - [8] M. Goldstein, *J. Chem. Phys.* **51**, 3728 (1969).
  - [9] S. Sastry, P. G. Debenedetti, and F. H. Stillinger, *Nature*

- 393**, 554 (1998).
- [10] G. Adam and J. H. Gibbs, J. Chem. Phys. **43**, 139 (1965).
  - [11] J. H. Gibbs and E. A. DiMarzio, J. Chem. Phys. **28**, 373 (1958).
  - [12] M. Mézard and G. Parisi, Phys. Rev. Lett. **82**, 747 (1999).
  - [13] T. R. Kirkpatrick, D. Thirumalai, and P. G. Wolynes, Phys. Rev. A **40**, 1045 (1989).
  - [14] J. P. Sethna, J. D. Shore, and M. Huang, Phys. Rev. B **44**, 4943 (1991).
  - [15] D. Kivelson *et al.*, Physica A **219**, 27 (1995).
  - [16] R. M. Ernst, S. R. Nagel, and G. S. Grest, Phys. Rev. B **43**, 8070 (1991).
  - [17] C. Dasgupta, A. V. Indrani, S. Ramaswamy, and M. K. Phani, Europhys. Lett. **15**, 307 (1991).
  - [18] N. Menon and S. R. Nagel, Phys. Rev. Lett. **74**, 1230 (1995).
  - [19] G. Parisi, in *Complex behaviour of glassy systems*, edited by M. Rubi and C. Perez-Vicente (Springer-Verlag, Berlin, 1997), pp. 111–121.
  - [20] J. Yvon, Suppl. Nuovo Cim. **9**, 144 (1958).
  - [21] E. R. Weeks *et al.*, Science **287**, 627 (2000).
  - [22] T. A. Weber and F. H. Stillinger, Phys. Rev. B **31**, 1954 (1985).
  - [23] W. Kob and H. C. Andersen, Phys. Rev. Lett. **73**, 1376 (1994).
  - [24] D. C. Rapaport, *The art of molecular dynamics simulation* (Cambridge University Press, New York, 1995).
  - [25] J.-L. Barrat, J.-N. Roux, and J.-P. Hansen, Chemical Physics **149**, 197 (1990).
  - [26] M. Toda, N. Saito, R. Kubo, and Hashitsume, *Statistical Physics II : Nonequilibrium Statistical Mechanics*, 2 ed. (Springer-Verlag, Berlin, 1991).
  - [27] J. P. Hansen and I. R. McDonald, *Theory of Simple Liquids*, 2 ed. (Academic Press, London, 1986).
  - [28] W. Kob and H. C. Andersen, Phys. Rev. E **52**, 4134 (1995).
  - [29] A. Rinaldi, F. Sciortino, and P. Tartaglia, Phys. Rev. B **63**, 061210 (2001).
  - [30] D. N. Perera and P. Harrowell, Phys. Rev. E **59**, 5721 (1999).
  - [31] M. A. DeBolt, A. J. Easteal, P. B. Macedo, and C. T. Moynihan, J. Am. Ceramic Soc. **59**, 16 (1976).
  - [32] F. H. Stillinger and T. A. Weber, Physical Review A **25**, 978 (1982).
  - [33] F. H. Stillinger and T. A. Weber, Science **225**, 983 (1984).
  - [34] W. H. Press, S. A. Teukolsky, W. T. Vetterling, and B. P. Flannery, *Numerical Recipes in C: The Art of Scientific Computing (2nd ed.)* (Cambridge University Press, Cambridge, UK, 1992), p. 420.
  - [35] C. A. Murray, private communication.
  - [36] R. N. Bhatt and A. P. Young, Phys. Rev. B **37**, 5606 (1988).
  - [37] L. P. Levy and A. T. Ogielski, Phys. Rev. Lett. **57**, 3288 (1986).
  - [38] L. Wu, Phys. Rev. B **43**, 9906 (1991).
  - [39] K. Hukushima and K. Nemoto, J. Phys. Soc. Japan **65**, 1604 (1996).
  - [40] K. Hukushima, H. Takayama, and H. Yoshino, J. Phys. Soc. Japan **67**, 12 (1998).
  - [41] W. Kob, C. Brangian, T. Stuhn, and R. Yamamoto, in *Computer Simulation Studies in Condensed Matter Physics XIII*, edited by D. P. Landau, S. P. Lewis, and H. B. Schuttler (Springer-Verlag, Berlin, 2001), p. 153.
  - [42] C. D. Michele and F. Sciortino, cond-mat **01112056**, (2001).